

Supporting information for

**A New Parameterization of Photolysis Rates for
Oxygenated Volatile Organic Compounds (OVOCs)**

Yuwen Peng ¹, Bin Yuan ^{1,*}, Sihang Wang ¹, Xin Song ¹, Zhe Peng ¹,
Wenjie Wang ², Suxia Yang ¹, Jipeng Qi ¹, Xianjun He¹, Yibo Huangfu ¹,
Xiao-Bing Li ¹, Min Shao ^{1,*}

¹ College of Environment and Climate, Institute for Environmental and Climate
Research, Guangdong-Hongkong- Macau Joint Laboratory of Collaborative Innovation
for Environmental Quality, Jinan University, 51143, China

² Multiphase Chemistry Department, Max Planck Institute for Chemistry, Mainz 55128,
Germany

**Correspondence to:* Bin Yuan (byuan@jnu.edu.cn) and Min Shao
(mshao@pku.edu.cn)

Section S1 Photolysis Reactions of OVOCs Covered in Current Atmospheric Chemistry Mechanisms

Based on years of related laboratory research, the current understanding of the photolysis rate constants for low-carbon OVOCs has become relatively well-established. These measurements have been documented in databases such as the MPI-Mainz UV/VIS (Keller-Rudek et al., 2013) IUPAC (Mellouki et al., 2021), and the NASA Chemical Kinetics and Photochemical Data for Use in Atmospheric Studies (Sander et al., 2011), as well as in associated literature (Calvert et al., 2011a). These databases include most of the photolysis rate constants reported in the literature, along with related parameters such as absorption cross-sections and quantum yields. Based on these data, photolysis rate constants for multiple OVOCs under clear-sky conditions can be calculated within models such as the TUV model (Madronich and Flocke, 1999), the Fast-J model (Wild et al., 2000), and the MCM detailed chemical mechanism (Jenkin et al., 2015). The TUV model includes 37 species and 47 reaction pathways, while the MCM mechanism includes 20 core species and 26 core reaction pathways. However, the species covered in these commonly used photolysis databases are mainly focused on single and bifunctional species containing 1 to 4 carbon atoms, with very few species of high-carbon-number or more complex functional group species (as shown in Table S4 and Figure S8).

The most widely used lumped chemical mechanisms in air quality models include the Carbon Bond Mechanism (CBM), the California State University Atmospheric Pollution Research Center Mechanism (SAPRC), and the Regional Atmospheric Chemistry Mechanism (RACM). For instance, the CB05 mechanism, in addition to the photolysis of inorganic compounds, only includes the photolysis of five species extracted from the IUPAC database (peroxynitrate, methyl hydroperoxide, formaldehyde, acetaldehyde, and PAN) and five classes of lumped species (organic nitrates, propionaldehyde and larger aldehydes, C3 and larger PANs, methylglyoxal and other aromatic compounds, and organic peroxides) (Yarwood et al., 2005).

With advances in measurement technology and deeper research in recent years, studies have revealed that many multifunctional OVOC species exhibit strong

46 photolysis (Clifford et al., 2011; Chen et al., 2011; Reed Harris et al., 2017; Liu et al.,
47 2018; Müller et al., 2014; Tomas et al., 2021). The photolysis of these high-carbon,
48 multifunctional species has become a weak link in quantifying the photolysis process
49 of OVOCs. However, the most recent measurement results have not been adequately
50 reflected in the parameterization methods of current atmospheric chemical mechanisms.
51 Therefore, there is an urgent need to integrate the latest measurement results to improve
52 the existing photolysis databases.

53

Section S2 Measurement Methods for Meteorological and Other Parameters

Meteorological parameters (temperature, pressure, relative humidity), photolysis rates, and trace gases including O₃, CO, SO₂, NO, and NO₂ were simultaneously measured at all three sites. O₃ was detected using a UV absorption analyzer (Thermo Scientific 49i, US), CO was measured using an infrared absorption analyzer (Thermo Scientific 48i, US), and SO₂ was monitored with a pulsed fluorescence analyzer (Thermo Scientific 43i-TLE, US). NO and NO₂ were determined using a chemiluminescence analyzer (Thermo Scientific 42i, US).

The photolysis rates of O₃, NO₂, HCHO, and HONO were measured using a photochemical flux spectrometer (PFS-100, Focused Photonics Inc., China). ClNO₂ and N₂O₅ were analyzed using an iodide time-of-flight chemical ionization mass spectrometry (Iodide-ToF-CIMS, Aerodyne Research Inc.) (Wang et al., 2020; Ye et al., 2021; Wang et al., 2022). At Guangzhou urban site, HONO was measured with a Long Path Absorption Photometer (LOPAP) (Yu et al., 2021), while at the PRD regional site, it was detected using a gas and aerosol collector (GAC) instrument (Yang et al., 2014). However, at the Beijing urban site, where HONO data were unavailable, it was estimated as 2% of NO₂ (Zhang et al., 2024).

Section S3 Dynamic Allocation Method for Semi-quantitative Concentrations from PTR-ToF-MS

To constrain as many intermediate species as possible in the atmosphere, this study applied an innovative dynamic allocation method to assign semi-quantitative concentrations to PTR-ToF-MS measurements. The PTR-ToF-MS measures a vast number of signals, some of which can be calibrated using a VOC gas standard or a liquid calibration unit. This allows for the determination of calibration factors, which relate the signals to the concentrations of the quantified species. The calibration factors for each species in PTR-MS are linearly proportional to the reaction rate constant k for the H_3O^+ proton transfer reaction. Therefore, a linear parameterization relationship can be constructed based on the calibration factors and reaction rate constants of the calibrated species, enabling the estimation of calibration factors for other uncalibrated compounds (Sekimoto et al., 2017; Wu et al., 2020). This method addresses the challenge of using mass spectrometry data to constrain explicit chemical mechanisms in models, particularly when isomers cannot be distinguished.

First, an observational-based box model was run for each site to provide a reference for the allocation. Most of the model settings are the same as in Scenario 2 described in the main text, with a time step of 5 minutes. The chemical mechanism used was MCM v3.3.1, with the additional photolysis mechanism for ClNO_2 . In this model, the concentrations of only 20 quantified VOC species were constrained (see Table S3). The simulation results are referred to as the base case.

Next, the concentrations of OVOCs at each time point in the model output were analyzed based on molecular formula. Using the base case output, the dynamic percentage contribution of OVOC species with the same molecular formula was calculated at each time step. Note that data for all constrained VOC species were excluded. For example, for the species with the molecular formula $\text{C}_2\text{H}_2\text{O}_3$ and a molecular mass of 74 g mol^{-1} , the results at the Guangzhou urban site corresponded to glyoxylic acid (HCOCO_2H) and formic anhydride (CHOOCHO) in the MCM, with average percentage contributions of 98% and 2%, respectively.

Finally, after filtering the PTR-ToF-MS data, real-time allocation was performed

102 based on the percentage contributions obtained in the previous step, constraining the
103 concentrations of additional intermediate species in Scenario 2. Fragment species,
104 species without oxygen atoms, and species whose molecular formulas did not overlap
105 with those in the MCM were removed. At this point, the PTR signal can be dynamically
106 allocated based on the simulation results from the base case (see Figure S9).

107 The same method was applied to three different sites in this study. At the
108 Guangzhou urban site, concentration for 212 different molecular formulas were
109 allocated to 1459 OVOCs in the MCM; at the Beijing urban site, concentration for 246
110 different molecular formulas were allocated to 1530 OVOCs in the MCM; and at the
111 PRD regional site, concentration for 220 distinct molecular formulas were allocated to
112 1172 OVOCs in the MCM.

Section S4 Incorporation of Photolysis Rate Data from Literature into the Database

If the literature reports the measured $j_{OVOC,overhead}/j_{NO_2,overhead}$ ratio, the ratio is directly incorporated into the database. If the reported value is the j_{OVOC} measured in a smog chamber, then the j_{OVOC}/j_{NO_2} under the same conditions is first calculated, and is converted to the ratio of $j_{OVOC,overhead}/j_{NO_2,overhead}$ before being added to the database. If the literature only provides the absorption cross-section and quantum yield for the species, the actinic flux is calculated using the TUV radiation model (Madronich and Flocke, 1999; Lantz et al., 1996) under conditions where SZA is 0° and altitude is 0 km. The $j_{OVOC,overhead}$ is then obtained by convolution according to Equation (1) and subsequently converted to $j_{OVOC,overhead}/j_{NO_2,overhead}$ before being added to the database (workflow shown in Figure S10).

Section S5 Calculation of reference value for various functional groups

Among the 109 species in the database, 64 species with single functional groups or combinations of functional groups were selected to provide measured data for the 21 classes of reference values. All data are presented in the form of j_{rel} ($= j_{OVOC,overhead}/j_{NO_2,overhead}$), making it easier for users to apply them to different environments. The absorption cross section data used in this section are sourced from the Mainz-MPI database (Keller-Rudek et al., 2013). Detailed information regarding the species used, j_{rel} values, number of carbon atoms, and other relevant data can be found in the supplementary table titled "*Species Used for RV*". The final corresponding reference values for the 21 classes containing 1 to 20 carbon atoms are provided in the supplementary table titled "*Reference Value Table*".

4.1 Aldehydes

(1) n-Aldehydes (CHO)

As the most extensively studied photodegradable OVOCs, the photolysis reference values for n-aldehydes containing 1 to 7 carbon atoms were obtained by averaging 20 reported values from the databases. The absorption cross-section of n-aldehydes with 1 to 7 carbon atoms is shown in Figure S11 (a). It can be observed that the absorption gradually increases from acetaldehyde (CH_3CHO) to propionaldehyde (C_2H_5CHO), while the absorption spectra of n-butyraldehyde ($n-C_3H_7CHO$) and n-pentanal ($n-C_4H_9CHO$) are almost identical. Therefore, for the aldehyde (-CHO) functional group, the average photolysis rate of n-aldehydes with 3 to 7 carbon atoms will be used as the reference value for the photolysis rate of aldehyde functional groups containing 8 or more carbon atoms (Figure S11 (b)). The photolysis reference value for aldehyde carbonyl groups containing 8 or more carbon atoms is $0.18\% \pm 0.053\% j_{NO_2}$.

(2) α , β -Unsaturated Aldehydes (UNCHO)

When a $C=C$ double bond appears between the α and β carbons of an aldehyde carbonyl group, a conjugated system is formed between the $C=O$ double bond and the $C=C$ double bond. Molecular theoretical calculations show that the formation of this conjugated system leads to a lowering of the energy level of the lowest unoccupied

molecular orbital (LUMO) and an increase in the energy level of the highest occupied molecular orbital (HOMO). This results in a reduction in the energy gap between the π and π^* orbitals, leading to a decrease in the transition energy and a red shift in the absorption wavelength (See Figure S12 (a)). This reduces the energy gap between the π and π^* orbitals, leading to a red shift in the absorption wavelength (Xu et al., 2013). Generally, as the conjugated chain lengthens, the red shift of the absorption peak is accompanied by an increase in absorption intensity.

Taking acrolein as an example, although its absorption intensity significantly increases due to the presence of the conjugated system, its quantum yield is notably lower than that of the corresponding aldehydes. This is because the acrolein molecule predominantly undergoes photolysis via a channel that results in the decomposition into one molecule of ethylene and one molecule of carbon monoxide (accounting for 40-60% of all photolysis pathways). Under standard atmospheric pressure, this reaction leads to significant quenching in the first excited state, resulting in a quantum yield of only about 0.0065 at 313 nm (Calvert et al., 2011a). Therefore, the increased absorption cross-section, combined with the low quantum yield, results in the photolysis rate of α , β -unsaturated aldehydes being significantly lower than that of saturated aldehydes. It should be noted that the α , β -unsaturated aldehydes discussed here contain only one C=C double bond and one aldehyde carbonyl group; dienal aldehydes containing two carbon-carbon double bonds will be discussed later. In the calculation of the photolysis rate for the unsaturated aldehyde (-UNCHO) functional group, the average photolysis rate of unsaturated aldehydes with 3-4 carbon atoms is used as the reference value for unsaturated aldehydes containing 5 or more carbon atoms (Figure S12 (b)), approximately $0.033\% \pm 0.014\% jNO_2$.

4.2 Ketones

(1) n-Ketones (CO)

The maximum absorption wavelength of n-alkyl ketones is primarily around 175 nm. When beyond 290 nm, it remains nearly unchanged regardless of the carbon number (Figure S13). Among n-alkyl ketones containing 1 to 4 carbon atoms, the

absorption cross section follows the order: pentanone > butanone > hexanone > propanone. Studies on the quantum yield of ketones are relatively limited. Only the quantum yield of acetone has a detailed calculation formula provided in the IUPAC recommendations, while the quantum yield of 2-butanone is assumed to be a constant 0.34 at 1 bar pressure. For ketones with methyl substitution, the IUPAC recommends a quantum yield of 1. Based on reported photolysis data for ketones, n-alkyl ketones exhibit photolysis rates that are approximately one order of magnitude lower than those of aldehydes. In the calculation of the reference value for the ketone (-C=O) functional group, the average photolysis rate of straight-chain ketones with 4 to 6 carbon atoms is used as the reference value for ketones containing 7 or more carbon atoms, approximately $0.029\% \pm 0.019\% jNO_2$ (Figure S15).

(2) Cyclic Ketones (CycloCO)

Cyclic ketones in the atmosphere originate from the oxidation of cyclic alkanes and are also directly released from anthropogenic sources (Calvert et al., 2011b). The absorption of cyclic ketones is influenced by their ring size. In terms of absorption cross section, cyclopropanone (containing 3 carbon atoms) exhibits the greatest maximum absorption wavelength (Figure S13). As the ring expands to cyclohexanone (containing 6 carbon atoms), the absorption undergoes a significant blue shift, accompanied by a notable reduction in intensity. Although cyclobutanone has a reported absorption cross-section of $2.17 \times 10^{-20} \text{ cm}^2 \text{ molecule}^{-1}$ only at 313 nm, it is still significantly lower than that of cyclopropanone. Combining the absorption cross-section data of cyclobutanone (Carless and Lee, 1972) and cyclopentanone (Nakashima et al., 1982) measured in cyclohexane solution, it is evident that cyclopropanone exhibits the strongest absorption above 290 nm among cyclic ketones. The absorption of cyclobutanone and cyclopentanone shift towards 290 nm, with a maximum absorption cross section of approximately $7.20 \times 10^{-20} \text{ cm}^2 \text{ molecule}^{-1}$. The absorption of cyclohexanone is similar to that of cyclopentanone, but its maximum absorption cross-section decreases to approximately $4.00 \times 10^{-20} \text{ cm}^2 \text{ molecule}^{-1}$. For cyclic ketones containing three carbon atoms, the photolysis rate of cyclopropanone ($3.4\% jNO_2$) is adopted as the reference value. For cyclic ketones with four or more

carbon atoms, the photolysis rate of cyclobutanone (0.24% jNO_2) is used as the reference value (Figure S15).

(3) Unsaturated Ketones (UNCO)

The estimation of reference values for unsaturated ketones is based on the photolysis frequencies of ketene ($CH_2=C=O$) and methyl vinyl ketone (MVK, $CH_3C(=O)CH=CH_2$). Ketene forms a new chromophore ($C=C=O$) compared to ketones, and its conjugated structure shifts the absorption cross section toward longer wavelengths due to a lower $n \rightarrow \pi^*$ transition energy, resulting in a maximum absorption wavelength greater than that of simple carbonyls (Figure S14). Its quantum yield remains above 0.9 between 290 nm and 320 nm and gradually declines to zero between 320 nm and 355 nm (Wade et al., 1997a; Wade et al., 1997b). The relatively high quantum yields above 290 nm leads to a rapid photolysis of approximately 2.6% jNO_2 , giving ketene an estimated photochemical lifetime of about one hour under midday sunlight. In comparison, replacing a methyl ($-CH_3$) group in acetone (CH_3COCH_3) with a vinyl group ($-CH=CH_2$) forms MVK, introducing a new chromophore that significantly increases its absorption wavelength and enhances its overlap with tropospheric actinic flux. At its maximum absorption wavelength, MVK's absorption cross section is 44% larger than that of acetone (Calvert et al., 2011b). However, despite this increase, MVK's quantum yield at 308 nm is only 0.16 and decreases with increasing wavelength, resulting in a lower photolysis rate compared to n -ketones (Gierczak et al., 1997). Due to the limited availability of quantum yield data for unsaturated ketones, the relative photolysis rate (j_{rel}) of MVK is currently used as the reference value for unreported unsaturated ketones, with an estimated value of $0.033\% \pm 0.014\% jNO_2$ (Figure S15).

4.3 Ortho-dicarbonyl Compounds

Ortho-dicarbonyl compounds refer to species in which two adjacent carbon atoms in the molecular structure are substituted with carbonyl groups. This category includes dialdehydes (e.g., glyoxal), aldehyde-ketone compounds (e.g., methylglyoxal), and diketones (e.g., 2,3-butanedione). In these compounds, the presence of two

chromophores on adjacent carbon atoms forms a conjugated system, where the interaction between the chromophores significantly alters the absorption spectrum compared to that of an isolated chromophore. The absorption in such conjugated systems cannot be simply regarded as the additive effect of two independent chromophores. Therefore, it is essential to classify and analyze different conjugated systems separately.

(1) Dialdehydes (OCHCHO)

Glyoxal (OCHCHO) is the structurally simplest α -dicarbonyl compound. As an important product of aromatic hydrocarbon oxidation, glyoxal plays a key role in atmospheric photolysis as a source of free radicals in the troposphere, contributing to both ozone formation and secondary organic aerosol (SOA) pollution (Rossignol et al., 2014; Tadić et al., 2006). The absorption cross section of glyoxal consists of two major absorption bands: a broad ultraviolet band between 220 to 350 nm and a stronger structured band in the 350 to 480 nm range (Figure S16 (a)). Methylglyoxal ($\text{CH}_3\text{C}(\text{O})\text{CHO}$), which contains one aldehyde carbonyl and one ketone carbonyl, exhibits a slightly lower absorption cross section than glyoxal, which contains two aldehyde carbonyls. However, methylglyoxal has a higher quantum yield above 290 nm compared to glyoxal (Figure S16 (b)), compensating for its lower absorption cross section. As a result, the photolysis rates of glyoxal and methylglyoxal are comparable, allowing them to be classified in one group for estimation. In the calculation of reference value for dialdehydes, the average photolysis frequency of glyoxal and methylglyoxal is used as the reference value for the photolysis rate of dialdehydes containing four or more carbon atoms (Figure S17), yielding an estimated value of $1.4\% \pm 0.046\% j\text{NO}_2$.

(2) Diketones (COCO)

For diketone compounds, the absorption cross section is slightly lower than that of methylglyoxal, and the maximum absorption wavelength exhibits a slight blue shift. The quantum yield of 2,3-butanedione ($\text{CH}_3\text{C}(\text{O})\text{C}(\text{O})\text{CH}_3$) is approximately 0.16 (Figure S16 (b)). However, there is significant disagreement in the literature regarding the photolysis rate of 2,3-butanedione (Figure S18), primarily due to variations in the

choice of cutoff wavelength. Although the quantum yield at longer wavelengths is relatively low, the absorption cross section remains substantial for wavelengths above 400 nm. Consequently, adjusting the cutoff wavelength from 492 nm to 410 nm results in a more than twofold decrease in the photolysis rate. Even when a theoretically higher quantum yield is considered, the derived photolysis rate remains lower than the values reported from observations (Klotz et al., 2001). Klotz et al. (2001) proposed the following relationship to estimate the photolysis rate of 2,3-butanedione under conditions of 0.5 km altitude and a total ozone column density of 350 DU:

$$j(\text{biacetyl}) = (0.0364 \pm 0.0026) \times jNO_2 - (3 \pm 11) \times 10^{-6} s^{-1}$$

According to this equation, at a solar zenith angle of 0° , the photolysis rate of 2,3-butanedione is approximately 3.6% jNO_2 . The relatively high observed photolysis rate may be attributed to the addition of HO_2 radicals to 2,3-butanedione molecules Calvert et al. (2011b), although considerable uncertainty remains. The photolysis rate range recommended by Calvert et al. (2011b) is represented by the gray dashed lines in Figure S18. The average value of the five reported data points within this range was used in this study as the photolysis rate of 2,3-butanedione, which is approximately 2.3% jNO_2 . The average photolysis frequency of 2,3-butanedione and 2,3-pentanedione is used as the reference value for the photolysis rate of diketones (Figure S17), yielding an estimated value of $2.9\% \pm 0.76\% jNO_2$.

(3) Unsaturated Dialdehydes (UNDICHO)

The estimation of reference photolysis values for unsaturated ketones is based on the photolysis frequencies of two unsaturated 1,4-dicarbonyl compounds, namely 2-butenedial ($HC(=O)CH=CHCH(=O)$) and 4-oxo-2-pentenal (acetyl acrolein, $O=CHCH=CHCH_2C(=O)H$). These compounds primarily originate from primary emissions or the ring-opening reactions of peroxy-bicyclic intermediates formed from the oxidation of aromatics. The strong absorption above 290 nm and the near-unity quantum yield result in rapid photolysis of the compound (Figure S19). Under boundary layer condition, photolysis serves as the dominant removal pathway for such compounds, with an estimated photochemical lifetime of approximately 10 to 15 minutes (Newland et al., 2019). The j_{rel} of 2-butenedial has been reported to be

approximately 14% jNO_2 , while the reported values for 4-oxo-2-pentenal vary across different studies, ranging from 5.7% jNO_2 to 21% jNO_2 (Iupac, 2012; Newland et al., 2019). The current implementation does not differentiate between Z and E configurations, this aspect could be integrated in later refinements. The average photolysis frequency of 2-butenedial and 4-oxo-2-pentenal has been adopted as the reference value for the photolysis rate of unsaturated dialdehydes, resulting in an estimated value of $12\% \pm 1.2\% jNO_2$ (Figure S20).

(4) Dienedials (DIENEDIAL)

Due to the similarity in absorption cross sections, 2,4-Hexadienal, which contains a single aldehyde carbonyl group, and 2,4-Hexadienedial, which contains two aldehyde carbonyl groups, are classified together in this estimation (Figure S19). E,E-2,4-Hexadienedial ($HC=OCH=CHCH=CHCH=O$) is a ring-opening product of aromatic hydrocarbon oxidation and contributes to both atmospheric oxidizing capacity and the formation of secondary organic aerosols (SOA) through photolysis (Klotz et al., 1999). The absorption characteristics of this compound are like those of other α , β -unsaturated aldehydes. However, the presence of four conjugated double bonds enhances its absorption strength and causes a stronger and redshifted absorption compared to simpler α , β -unsaturated aldehydes. The j_{rel} of E,E-2,4-Hexadienedial is reported to be around 2.1% jNO_2 (Klotz et al., 1999; Xiang and Zhu, 2007), while that of 2,4-Hexadienal averages 2.6% jNO_2 . The reference value for dienedial compounds is determined to be $2.2\% \pm 0.31\% jNO_2$ (Figure S20).

4.4 N-Containing Compounds

A variety of nitrogen-containing OVOCs are present in the atmosphere. These compounds may be directly emitted, including amides commonly used as solvents in industrial processes (Tuazon et al., 1994) and emissions originating from diesel engines (Simpson et al., 2002). In addition, nitrogen-containing OVOCs can be formed through secondary formation in the atmosphere, such as intermediates generated during the atmospheric degradation of amines (Finlayson-Pitts and Pitts Jr, 1999). Alkyl nitrates ($RONO_2$), alkyl nitrites ($RONO$), and peroxyacetyl nitrate (PAN) can also be formed

through the reactions of alkoxy radicals ($\text{RO}\bullet$) or alkyl peroxy radicals ($\text{RO}_2\bullet$) with NO or NO_2 (Calvert et al., 2002). Organic nitrates can serve as reservoir species for NO_x in the atmosphere, thereby influencing the regional nitrogen oxide budget (Bertram et al., 2013) and subsequently affecting the formation of ozone (Aruffo et al., 2014) and SOA (Kiendler - Scharr et al., 2016).

(1) Alkyl Nitrates (ONO_2)

In the tropospheric solar wavelength range ($>290\text{ nm}$), the primary photolysis pathway for alkyl nitrates leads to the formation of $\text{RO}\bullet$ radical and NO_2 . Alkyl nitrates, alkyl dinitrates, peroxy nitrates, and PANs share similar absorption cross-sections (Figure S21), with weak absorption above 290 nm , resulting in low photolysis rates. It is generally assumed that the quantum yield of all alkyl nitrates is close to 1, an estimate that aligns well with observations for most compounds except methyl nitrate (CH_3ONO_2). The measured photolysis rate of CH_3ONO_2 differs by a factor of three from the estimated value assuming a quantum yield of 1. This discrepancy is likely due to the strong temperature dependence of CH_3ONO_2 's absorption cross section, which requires further experimental validation (Calvert et al., 2011b). To account for this, the current estimation adopts a lower photolysis rate for CH_3ONO_2 , consistent with the IUPAC recommended value of approximately $1.1\% j\text{NO}_2$. Although the photolysis rate of alkyl nitrates shows a slight increasing trend with carbon number, a linear fit would result in over-extrapolation for higher-carbon species. Given the overall weak photolysis of alkyl nitrates, the average photolysis frequencies of compounds containing 1 to 5 carbon atoms is used as the reference value for unmeasured alkyl nitrates, yielding an estimated value of $0.019\% \pm 0.0032\% j\text{NO}_2$ (Figure S23).

(2) Peroxy Nitrates (COOONO_2)

In the database, compounds classified under this category include Peroxyacetyl Nitrate (PAN) and Peroxypropionyl Nitrate (PPN). PAN and PPN exhibit weak solar absorption within the troposphere (Figure S21) and are primarily removed in the lower troposphere through unimolecular decomposition and ultraviolet photolysis. The j_{rel} of PAN has been reported to be around $0.0082\% j\text{NO}_2$ under overhead sun condition, corresponding to a photochemical lifetime of approximately 13 days. The j -value of

PPN is about 1.7 times that of PAN, resulting in a photochemical lifetime of approximately 7.3 days. The reference photolysis value for peroxyacyl nitrates is determined as the average of PAN and PPN, yielding an estimated value of $0.011\% \pm 0.0041\% jNO_2$ (Figure S23).

(3) Carbonyl Nitrates (COONO₂)

As products of chain-terminating reactions in the tropospheric HO_x and NO_x catalytic cycles, organic nitrates (RONO₂) affecting the local ozone formation. Among them, carbonyl nitrates constitute a significant fraction of the total RONO₂ pool, particularly in regions dominated by biogenic NMVOC emissions. Due to their relatively long atmospheric lifetimes, carbonyl nitrates can undergo long-range transport, impacting atmospheric chemistry on a regional scale (Beaver et al., 2012). Müller et al. (2014) re-evaluated the key kinetic parameters of organic nitrates and reported photolysis rates for six carbonyl nitrates, covering species with 2 to 5 carbon atoms. The reported j_{rel} range from $0.19\% jNO_2$ to $1.5\% jNO_2$, corresponding to atmospheric lifetimes from 1.7 to 13 hours. Compared to alkyl nitrates, carbonyl nitrates exhibit a redshifted absorption spectrum with slightly stronger absorption, coupled with a near-unity quantum yield (Figure S22). As a result, their photolysis rates are significantly higher than those of alkyl nitrates. Note that this evaluation applies only to compounds containing one ketone carbonyl and one nitrate functional groups. The effects of aldehyde carbonyl substitution, unsaturation, ring structures, and hydroxyl substitution will be discussed separately in Section S6 on adjustment coefficients. The reference photolysis value is determined as the average photolysis rate of carbonyl nitrates containing 3 to 5 carbon atoms, yielding an estimated value of $0.47\% \pm 0.074\% jNO_2$ (Figure S23).

(4) Alkyl Nitrites (ONO)

Alkyl nitrites (–ONO) in the troposphere primarily originate from the reaction of alkoxy radicals (RO•) with nitric oxide (NO), serving as temporary sinks for atmospheric NO_x (Calvert et al., 2011b). These compounds undergo rapid photolysis under sunlight, generating RO• and NO, thereby driving the ozone formation in troposphere. Compared to alkyl nitrates, alkyl nitrites exhibit a greater spectral overlap

with solar radiation at tropospheric wavelengths (>290 nm), indicating stronger absorption (Figure S24).

Methyl nitrite has the strongest absorption and a near-unity quantum yield, leading to a significantly higher photolysis rate than other alkyl nitrites (Figure S25). The absorption cross sections of alkyl nitrites containing 2 to 4 carbon atoms are highly similar. Though, for propyl nitrite and butyl nitrite, a significant decrease in absorption cross-section is observed beyond 335 nm. The data for these two compounds were inferred from published graphical data measured in liquid hexane, combined with a single-wavelength gas-phase absorption cross-section measurement at 366 nm and can be uncertain. For n-alkyl nitrites containing 2 to 4 carbon atoms, the reported quantum yields range from 0.24 to 0.36, leading to an atmospheric photolysis lifetime of approximately 22 to 33 minutes (Calvert et al., 2011b). Based on trends observed in other compounds, tert-butyl nitrite may exhibit a higher quantum yield, resulting in faster photolysis. Due to the lack of sufficient data, the current parameterization does not differentiate the effects of isomerism on the photolysis rate of alkyl nitrites. The reference value for alkyl nitrites is determined as the average for alkyl nitrites containing 2 to 4 carbon atoms, yielding $5.4\% \pm 1.5\% jNO_2$ (Figure S25).

(5) N-Nitrosamine (NNO)

Nitrosamines are one of the degradation products of amines and are potentially carcinogenic (Nielsen et al., 2012). The nitrosamine functional group exhibits a characteristic $n \rightarrow \pi^*$ electronic transition, with a quantum yield near unity at 363.5 nm (Geiger et al., 1981). As a result, nitrosamines undergo rapid photolysis under sunlight. Nielsen et al. (2012) summarized photolysis rates for nine different N-nitrosamines containing 2–5 carbon atoms, concluding that the photolysis rate for nearly all nitrosamines is approximately $34\% \pm 3.0\% jNO_2$. Such rapid photolysis leads to an atmospheric removal time of approximately 30 minutes. The average photolysis rate for N-nitrosamines containing 2 to 5 carbon atoms has been used to estimate the photolysis rate for unmeasured N-nitrosamines, yielding a reference value of $32\% \pm 0.93\% jNO_2$ (Figure S25). Currently, the chemical reactions related to N-nitrosamine have not yet been included in the MCM v3.3.1 mechanism.

4.5 Aromatic Compounds

During the oxidation of aromatics, the addition of different functional groups to the benzene ring introduces new absorption bands, shifting absorption towards longer wavelengths. This increases spectral overlap with tropospheric solar radiation, enhancing the potential for photolysis (Figure S26). In the database, four classes of compounds are included for reference value calculations: nitrobenzaldehydes, nitrobenzenes, aromatic aldehydes, and nitrophenols.

While nitrobenzaldehyde and nitrobenzene exhibit similar absorption cross sections, their quantum yields differ significantly. Nitrobenzaldehyde has a quantum yield of about 0.5, whereas nitrobenzene's quantum yield is only 3.5×10^{-3} (inferred from measured solution-phase quantum yields of nitro-naphthalene). As a result, nitrobenzaldehyde has an average j_{rel} of 48% jNO_2 , whereas nitrobenzene's is only 0.19% jNO_2 .

For aromatic aldehydes, the available benzaldehyde quantum yield data cannot fully explain the observed high photolysis rates, indicating the need for further investigation (Calvert et al., 2011b). In the current study, a higher reported photolysis frequency of approximately 1.8% jNO_2 is adopted. Although nitrophenols exhibit much stronger absorption compared to the other three kinds of compounds, their quantum yield is only around 1.2×10^{-3} (Chen et al., 2011), resulting in a j_{rel} of 1.3% jNO_2 and an atmospheric photolysis lifetime of approximately 2 hours.

The measured photolysis rates and reference values for these four classes of compounds are presented in Figure S27. Overall, significant challenges remain in the photolysis parameterization of aromatic compounds, including discrepancies between observations and known parameters, large variations in reported photolysis values, and a lack of gas-phase experimental data. These issues require further refinement and optimization in future studies.

4.6 Other Compounds

(1) Keto Acids (COCOOH)

A typical representative of keto acids is pyruvic acid, a common organic acid

widely present in plants and tropospheric air with significant BVOC emissions (Eger et al., 2020). Structurally, pyruvic acid can be considered as acetone with one methyl group replaced by a carboxyl group ($-\text{C}(=\text{O})\text{OH}$), forming a new chromophore ($-\text{C}(=\text{O})\text{C}(=\text{O})\text{OH}$). This replacement shifts the absorption spectrum toward longer wavelengths (Figure S28), increasing the maximum absorption wavelength from below 290 nm to 350 nm (Calvert et al., 2011b).

Due to the lack of reliable quantum yield data, reported photolysis frequencies for pyruvic acid vary significantly across studies. Eger et al. (2020) measured a photolysis frequency of $0.37\% jNO_2$ in northern boreal forest, whereas Calvert et al. (2011b) estimated j_{rel} ranging from $1.1\% jNO_2$ to $3.9\% jNO_2$, depending on different quantum yield assumptions. In this study, the average reported value of $1.8\% \pm 1.6\% jNO_2$ was adopted as the reference value for all keto acids (Figure S29). Note that only compounds containing the full chromophore structure ($-\text{C}(=\text{O})\text{C}(=\text{O})\text{OH}$) are classified as keto acids. Compounds with isolated ketone ($-\text{C}(=\text{O})-$) and carboxyl ($-\text{C}(=\text{O})\text{OH}$) groups are not included in this category.

(2) Hydroperoxides (COOH)

Hydroperoxides are a class of compounds characterized by the hydroperoxy group ($-\text{OOH}$), including methyl hydroperoxide (CH_3OOH) and hydroxymethyl hydroperoxide (HOCH_2OOH). The photolysis of CH_3OOH produces CH_3O and OH radicals, but its photolysis rate is relatively low, making only a limited contribution to the total OH budget (Calvert et al., 2011b). Currently, photolysis data are only available for one-carbon hydroperoxides. As a result, the reference photolysis value is determined as $0.056\% \pm 0.0014\% jNO_2$, the same as methyl hydroperoxide (Figure S29). Although absorption enhancement with increasing carbon chain length is a possibility, there is currently insufficient data to confirm this assumption. Further measurements are needed to refine the parameterization for larger hydroperoxides.

(3) Peroxy acids (COOOH)

In the atmosphere, HO_2 radicals react with peroxyacyl species, leading to the formation of significant amounts of carboxylic and peroxy-carboxylic acids (Orlando and Tyndall, 2003). In addition to secondary formation, direct emissions of peracetic

acid have been reported in certain scenarios, such as during the use of disinfectants in building disinfection events (Ding et al., 2025). Carboxylic acids do not absorb above 290 nm and are therefore not considered for photolysis. However, peroxy-carboxylic acids exhibit a redshift in their absorption spectrum, making photolysis possible in the troposphere, despite their weak absorption (Figure S28). For all peroxy acids, the reference photolysis value is assumed to be the same as that of peracetic acid, estimated at 0.0085% jNO_2 (Figure S29).

Section S6 Calculation of adjustment coefficients for various functional groups

To enhance the flexibility and accuracy of the parameterization while maximizing the utilization of data available in the database, 10 adjustment coefficients have been introduced. Unlike the single-chromophore species discussed in Section S5, the species considered here involve multiple chromophores that interact with each other. The adjustment program serves as a correction module applied to the reference value (RV) after the main program has identified the functional groups and retrieved their respective reference values. The derivation of these parameters is primarily based on direct inferences from the relationships between photolysis rates of different species. Whenever available, absorption cross-section and quantum yield data are also considered. The dataset used to summarize these parameters can be found in the supplementary table titled "*Species Used for Coeff*".

5.1 Branched aldehydes

Branched aldehydes can be considered as derivatives of straight-chain aldehydes with methyl ($-\text{CH}_3$) substitutions along the carbon chain. In terms of absorption cross sections, no significant differences are observed between isopentaldehyde ($\text{i-C}_5\text{H}_{11}\text{CHO}$) and n-pentanal, or between isobutyraldehyde ($\text{i-C}_3\text{H}_7\text{CHO}$) and n-butanal (Figure S30). However, 2,2-dimethylpropanal ($\text{t-C}_5\text{H}_{11}\text{CHO}$) exhibits a significantly lower absorption cross section compared to n-pentanal, resembling that of acetaldehyde. This suggests that pivalaldehyde may represent a unique case. For most branched aldehydes, structural isomerism has a negligible impact on their absorption cross sections. Among the few available quantum yield reports for aldehydes, isomerization appears to significantly enhance the quantum yield of these species. The quantum yield of $\text{i-C}_3\text{H}_7\text{CHO}$ is reported to be approximately 1, whereas that of n-butanal is only 0.31. Consequently, the photolysis rate of isobutyraldehyde is nearly three times that of n-butanal.

Although no quantum yield data are available for $\text{t-C}_5\text{H}_{11}\text{CHO}$, its absorption cross section is similar to that of acetaldehyde, yet its photolysis rate is nearly four times higher. This suggests that the significantly higher photolysis rate of $\text{t-C}_5\text{H}_{11}\text{CHO}$ is

primarily driven by a substantially greater quantum yield compared to acetaldehyde. Such an inference aligns with previous studies, which have suggested that branched aldehydes undergo more pronounced photolysis compared to their linear counterparts (Calvert et al., 2011a). Therefore, in the parameterization, the adjustment coefficient of the carbonyl functional group in branched aldehydes is calculated using data from n-butanal and isobutyraldehyde. The adjustment coefficient is determined as $RV_i \times 3.1$.

5.2 Branched ketones

Another example is the analysis of branched ketones. Branched ketones can be regarded as ketones with methyl ($-\text{CH}_3$) substitutions at different positions along the carbon chain. The absorption characteristics of branched ketones are similar to those of straight-chain ketones, with the only notable exception being 2,4-dimethyl-3-pentanone, which exhibits slightly stronger absorption (Figure S31). Through the comparison of j_{rel} , it can be observed that methyl substitution at the β -position of 2-pentanone (forming 4-methyl-2-pentanone) results in an enhancement of absorption and an increase in the j_{rel} by 0.23% $j\text{NO}_2$. Similarly, methyl substitution at the γ -carbon of 2-hexanone (forming 5-methyl-2-hexanone) leads to an 0.15% $j\text{NO}_2$ increase in the j_{rel} . When both α -carbon positions of 3-pentanone are substituted with methyl groups (forming 2,4-dimethyl-3-pentanone), the absorption is significantly enhanced (due to the lack of photolysis data for 3-pentanone, 2-pentanone is used as a surrogate here). This effect may be attributed to an alkyl-induced red shift in absorption, leading to a 0.36% $j\text{NO}_2$ increase in the j_{rel} . Compared to the reference value of corresponding number of carbons, it can be inferred that methyl substitution at the β - or γ -carbon increases the photolysis rate of straight-chain ketones by approximately 0.18% $j\text{NO}_2$, whereas methyl substitution at both α -carbons enhances the photolysis rate by approximately 0.35% $j\text{NO}_2$.

5.3 Hydroperoxides

Hydroxyl substitution causes a blue shift in the absorption of methyl hydroperoxide, leading to a slight reduction in its photolysis rate. Therefore, the adjustment coefficient for hydroxyl substitution on hydroperoxides is $RV_i \times 0.96$.

5.4 Carbonyl Nitrates

(1) Aldehyde carbonyl substitution

Nitroxy ethanal ($\text{HC(=O)CH}_2\text{ONO}_2$) has a j_{rel} of $1.5\% j\text{NO}_2$, which is significantly higher than the j_{rel} of $0.47\% j\text{NO}_2$ observed for other ketone-carbonyl nitrates (Figure S23). Based on the comparison between nitroxy ethanal and the reference value of COONO_2 containing two carbon atoms, the adjustment coefficient for aldehyde-carbonyl substitution on ketone-carbonyl nitrates is determined to be $RV_i \times 3.2$.

(2) Ring substitution

Cyclo nitrates, such as cyclopentyl nitrate, exhibit absorption at similar wavelengths as other nitrates but with weaker absorption cross sections. Although the absorption cross section data for 2-nitrooxy cyclohexanone is not yet available, it can be inferred that the cyclic structure and the carbonyl nitrate functional group interact antagonistically, leading to a reduction in photolysis frequency. This inference aligns with the j_{rel} comparison results, where the reference value of COONO_2 containing six carbon atoms is $0.47\% j\text{NO}_2$, whereas 2-nitrooxy cyclohexanone has a lower value of only $0.20\% j\text{NO}_2$. Therefore, the adjustment coefficient for ring substitution on carbonyl nitrates is determined to be $RV_i \times 0.43$.

(3) Hydroxyl group substitution

Nitrooxy enal refers to an organic compound that contains both a nitrooxy ($-\text{ONO}_2$) functional group and an enal ($-\text{C(=O)-CH=CH}_2$) group. Through the oxidation of isoprene by NO_3 , the first-generation nitrate 3-methyl-4-nitroxy-2-butenal (NC_4CHO , $\text{OCHCH=C(CH}_3\text{)CH}_2\text{ONO}_2$) is formed. Compared to carbonyl nitrates, this structure includes an adjacent C=C double bond, which significantly enhances the absorption of the molecule, thereby promoting photolysis. This effect is evident from the j_{rel} of NC_4CHO , which is $5.6\% j\text{NO}_2$, significantly higher than reference value of COONO_2 containing 5 carbon atoms after aldehyde carbonyl substitution ($1.8\% j\text{NO}_2$). Based on this comparison, the adjustment coefficient for this case is determined to be $RV_i \times 3.2$.

5.5 Alkyl Nitrates

(1) Alkyl dinitrates

Dinitrates are important products formed from the reaction of NO_3 radicals with unsaturated hydrocarbons, playing a significant role in atmospheric chemistry. Photolysis serves as the primary removal pathway for saturated dinitrates in the atmosphere (Barnes et al., 1993). Although the UV spectra of nitrates are generally similar, dinitrates exhibit a red-shifted absorption compared to alkyl nitrates, extending into the spectral range of atmospheric interest (Figure S32). The presence of two $-\text{ONO}_2$ groups in dinitrates enhances absorption, resulting in a photolysis rate higher than the simple sum of the reference values for two $-\text{ONO}_2$ groups. In this study, the photolysis frequencies of 1,2-propanediol dinitrate, 1-butyl nitrate, and 2-butyl nitrate were used. A linear regression was performed using the photolysis frequencies of dinitrates and the corresponding alkyl nitrates (after multiplying by two to account for the additional nitrate group), resulting a slope of 3.1. Thus, for dinitrates, in addition to multiplying by the number of functional groups, the reference value needs to be further adjusted as $RV_i \times 3.1$.

(2) Ring substitution

The absorption cross section of cyclopentyl nitrate is slightly lower than that of 2-pentyl nitrate and 3-pentyl nitrate, showing a more rapid decline at wavelengths greater than 290 nm (Figure S32). The j_{rel} of cyclopentyl nitrate is 0.0083% j_{NO_2} , which is significantly lower than the reference value of ONO_2 containing five carbon atoms (0.023% j_{NO_2}). Therefore, the adjustment coefficient for ring substitution on alkyl nitrates is determined to be $RV_i \times 0.35$.

(3) Hydroxyl group addition

After the addition of a hydroxyl group, the absorption cross section of 2-nitrooxy ethanol is reduced compared to ethyl nitrate, with a blue shift in absorption (Figure S32), leading to a decrease in photolysis rate. The adjustment coefficient for hydroxyl group addition is determined to be $RV_i \times 0.057$.

Section S7 Calculation of adjustment coefficients for various functional groups

In addition to the 2327 photodegradable species already included in the MCM mechanism, this study identifies an additional 714 species with photodegradable functional groups. The photolysis rates of these reactions are estimated using a parameterization method, while the photolysis products are substituted by products from structurally similar species. The degree of unsaturation (DoU) of all additional photodegradable species was first calculated. The Degree of Saturation (DoU) is a concept often used in atmospheric chemistry to represent the extent to which a molecule is saturated with functional groups, such as nitrogen (N), oxygen (O), or other atoms. Based on the structure of the species (such as whether it contains nitrogen atoms, whether it has a ring structure), and its DoU, similar species from the existing MCM reactions were identified, and the same products were adopted. Generally, the photolysis products consist of one or two radicals. If no similar structure is found, the species photolysis into the simplest RO₂ radicals (such as CH₃O₂). This rough product estimation was defined to ensure the accuracy of the number of radicals generated during photolysis. However, it is an over-simplified approach and may have issues such as carbon loss in the mechanism, which needs to be optimized in future research. The specific species classification and surrogate photolysis products are provided in Table S5.

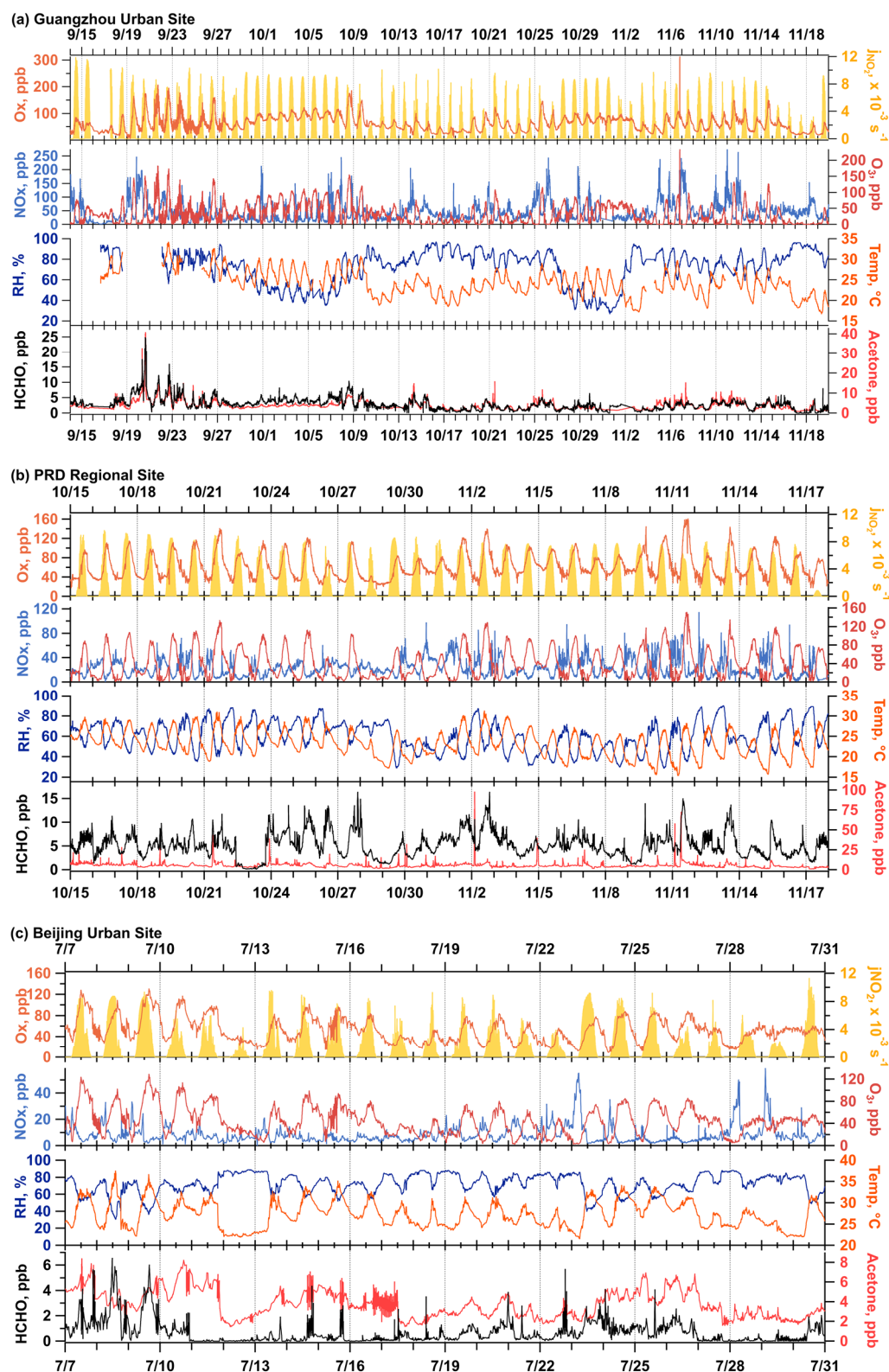


Figure S1 Time series of Ox (define as $O_3 + NO_2$), j_{NO_2} , NOx, ozone (O_3), relative humidity (RH), temperature (Temp), formaldehyde (HCHO), and Acetone during the campaign of the Guangzhou urban site (a), the PRD regional site (b), and the Beijing urban site (c). All data presented here are the average of every 5 minutes.

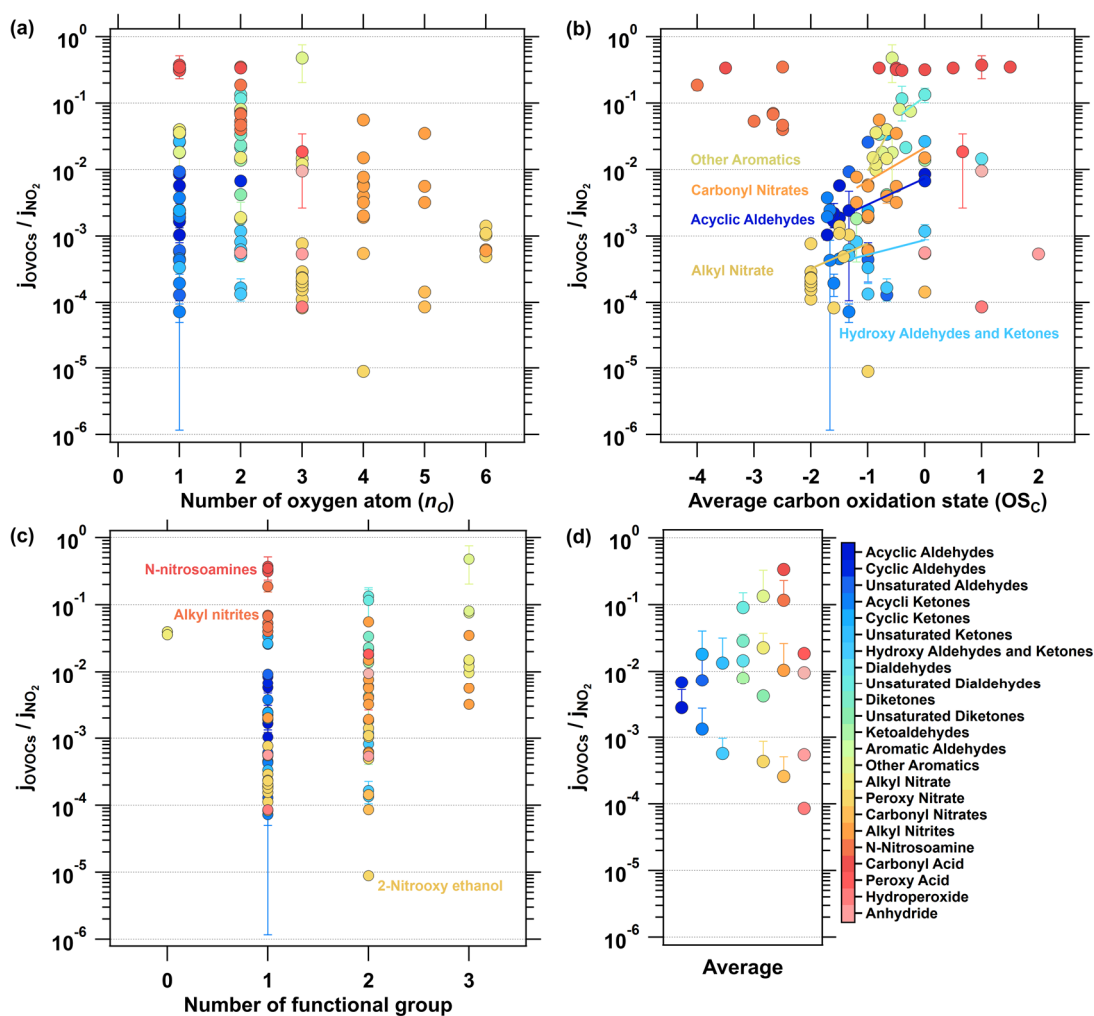


Figure S2 Relationships between the relative photolysis rates of various OVOCs and the number of oxygen atoms (a), average carbon oxidation state (b), and functional groups (c) they contain. The average relative photolysis rates are illustrated in panel (d), where only positive error bars are displayed.

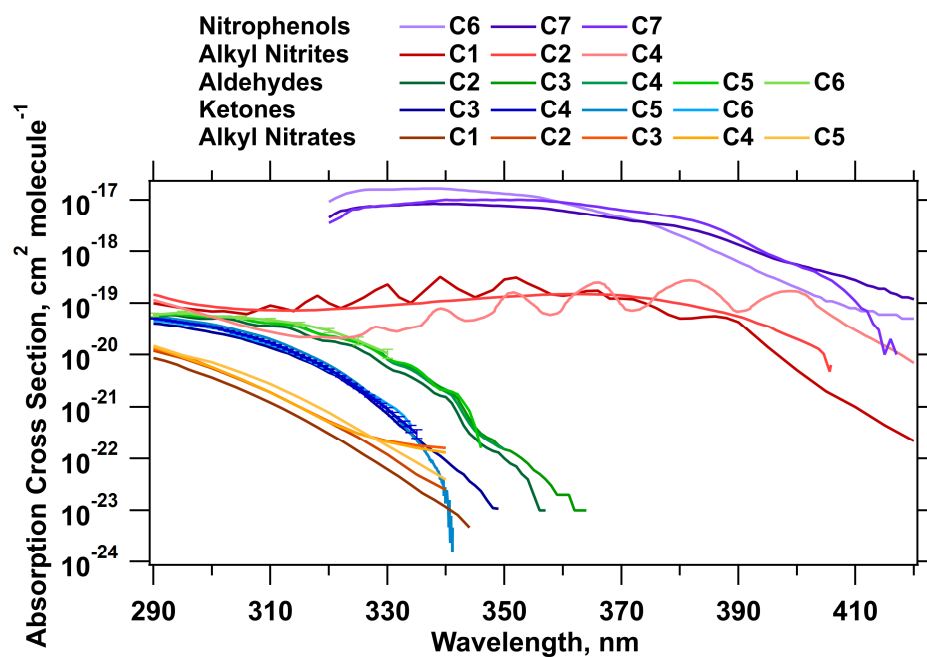


Figure S3 Relationship between absorption cross-sections and wavelengths for different family of compounds. The lines with similar colors in the figure represent compounds with the same functional group but different carbon numbers. The absorption cross-sections data are sourced from The MPI-Mainz UV/VIS Spectral Atlas of Gaseous Molecules of Atmospheric Interest (Keller-Rudek et al., 2013).

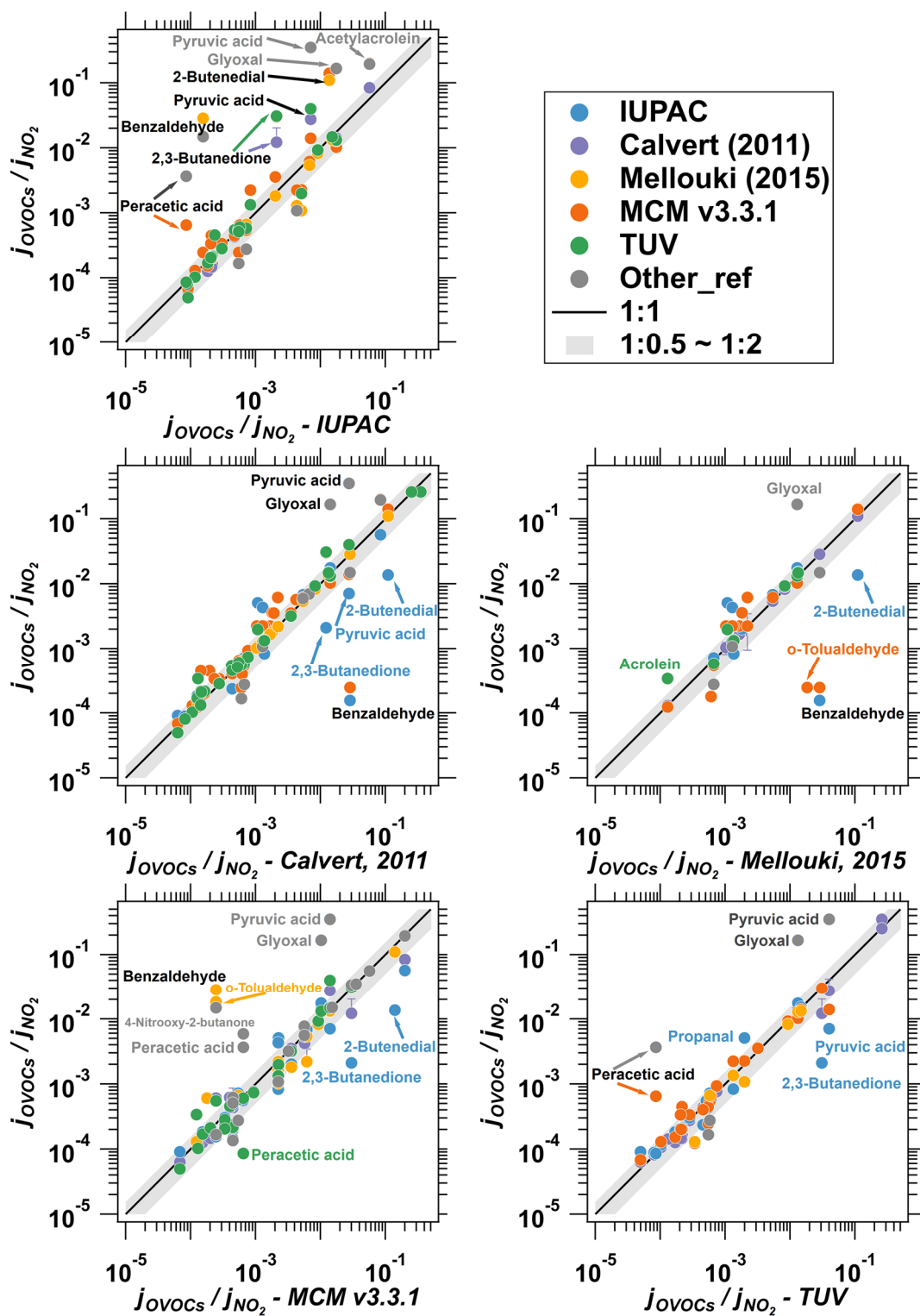


Figure S4 Comparison of j_{rel} from different sources in the photolysis database. The black line indicates the 1:1 agreement and the gray band represents deviation of a factor of 2.

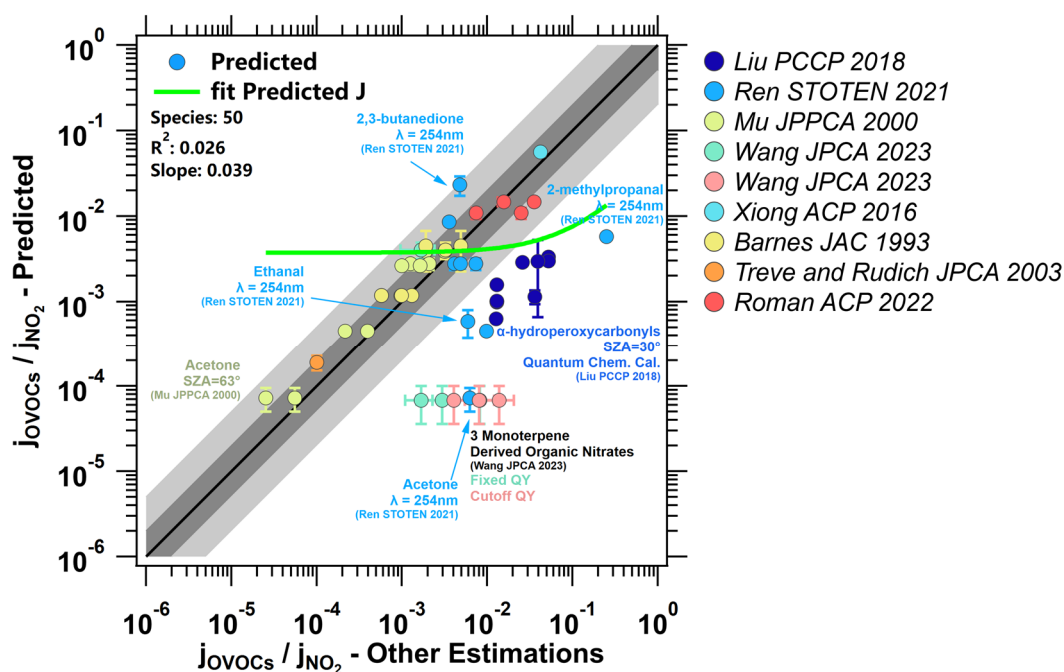


Figure S5 Comparison of predicted j_{rel} with the comparison group. Each point corresponds to a specific compound, with species showing larger deviations labeled for clarity. The green curve represents the fitted prediction. The black line indicates the 1:1 agreement and the darker gray band represents deviation of a factor of 2, while the lighter gray band extends to deviation for a factor of 5.

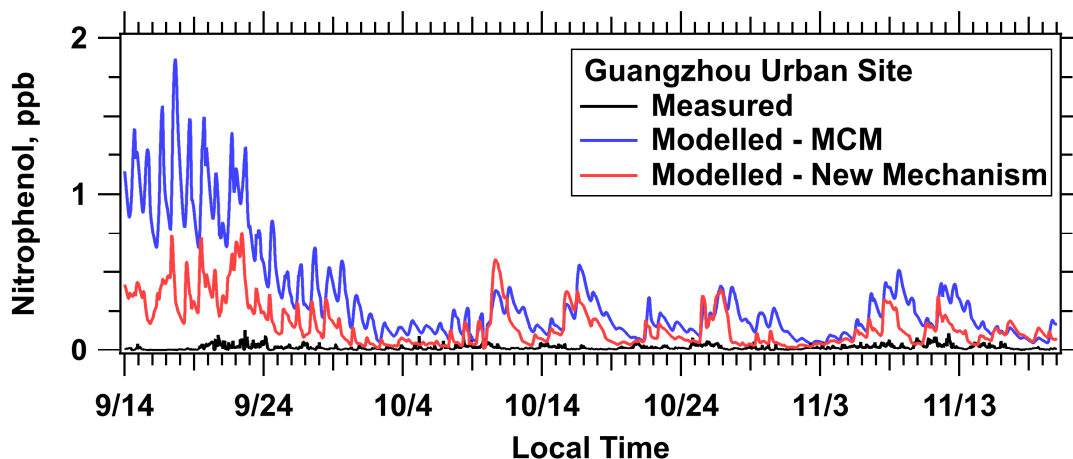
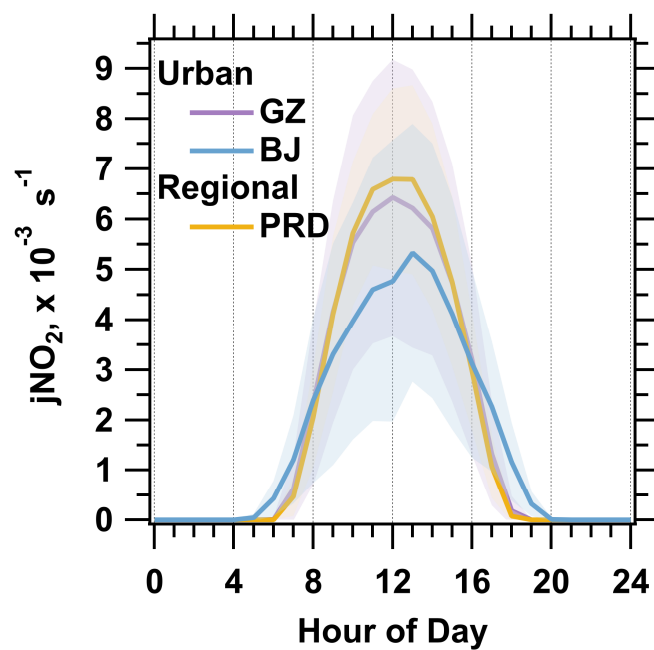


Figure S6 Comparison of modelled and measured nitrophenol concentrations of Guangzhou urban site in Scenario 1. The black line represents PTR-measured concentrations, the blue line denotes simulations using the MCM V3.3.1 mechanism, and the red line corresponds to simulations incorporating the new photolysis mechanism. The Root Mean Square Error (RMSE) of the MCM simulation is 0.4537, with an Index of Agreement (IOA) of 0.0373. With the new photolysis mechanism, RMSE decreases to 0.1973, and IOA increases to 0.0935, indicating reduced error and improved model performance.



667

668 **Figure S7** Diurnal variation of jNO_2 at three sites during the campaign. The purple
 669 line represents the Guangzhou urban site, the blue line represents the Beijing urban site,
 670 and the yellow line represents the PRD regional site. The shaded areas in corresponding
 671 colors indicate the standard deviation.

672

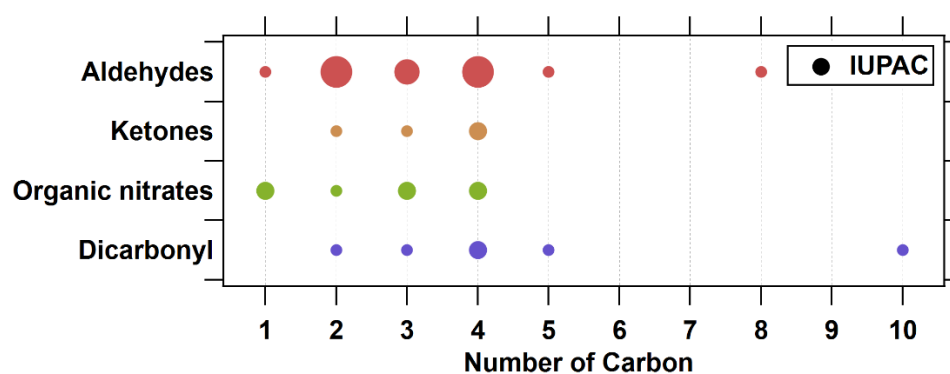


Figure S8 Carbon number distribution of typical OVOCs in the IUPAC database. The size of the dots represents the quantity of species, with the smallest dots indicating one species and the largest dots indicating four species.

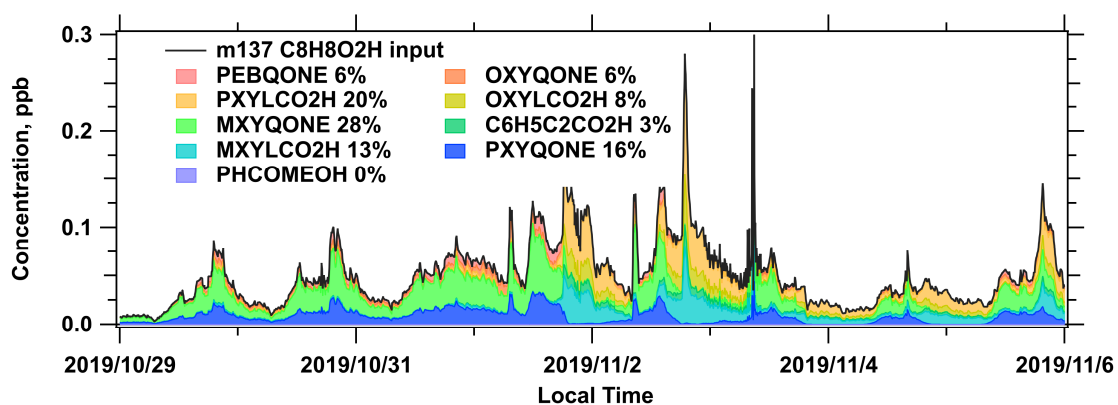


Figure S9 Example of one of the allocation results for PTR-ToF-MS semi-quantitative concentrations. The black line represents the concentration data obtained from PTR-ToF-MS measurements, while the colored shaded areas indicate the concentrations of different MCM species. The species names in the legend are followed by the average percentage contribution throughout the entire campaign at the Guangzhou urban site.

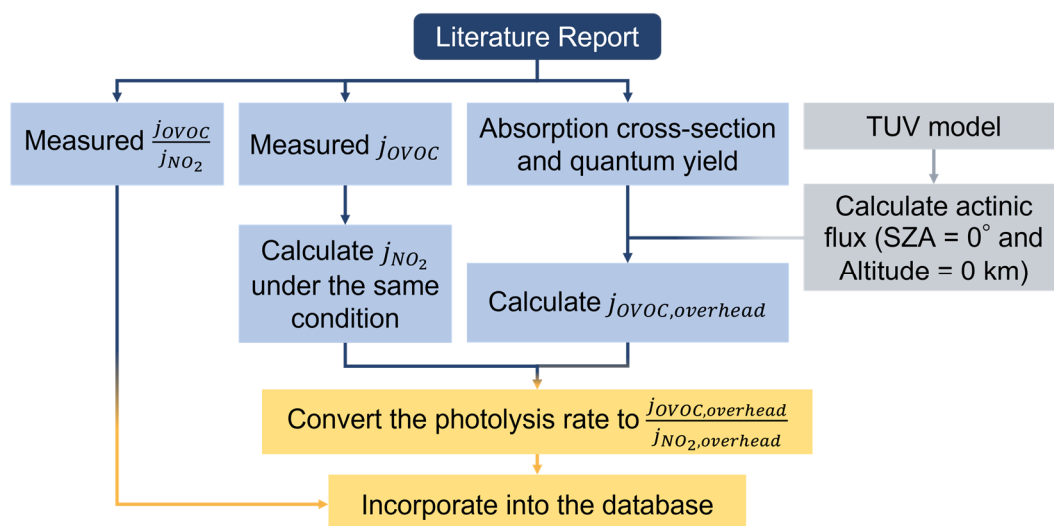


Figure S10 Workflow for processing literature data into photolysis database

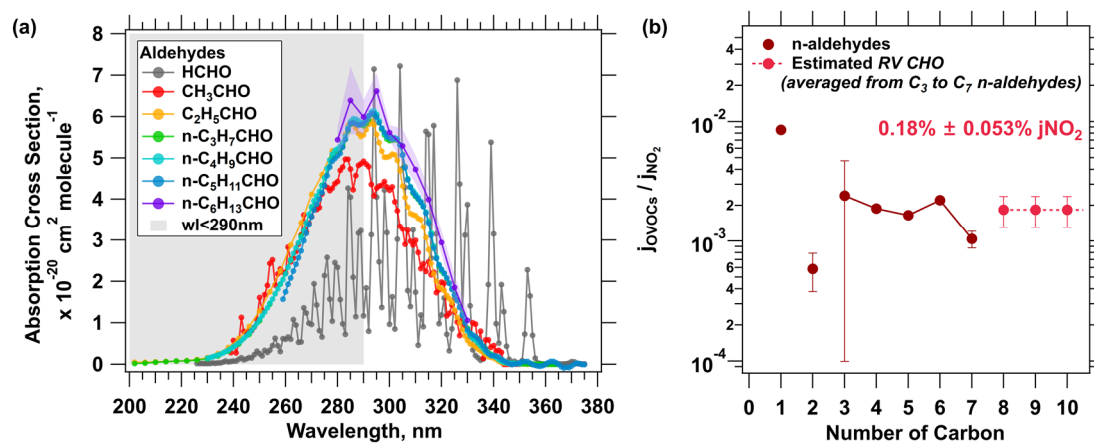


Figure S11 Absorption cross-sections of n-aldehydes (a) and the ratio of photolysis rates of n-aldehydes to NO₂ (b).

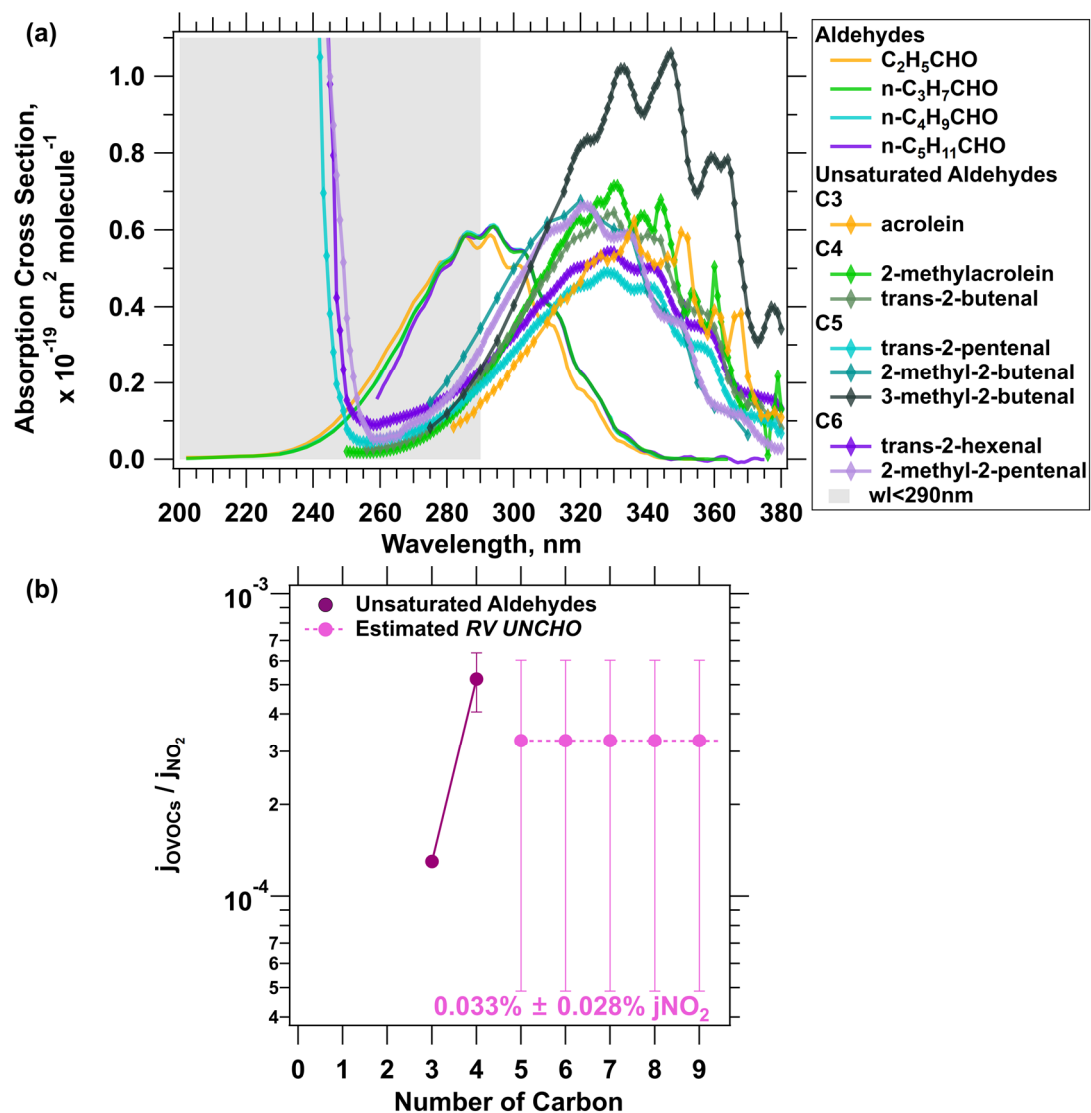


Figure S12 Absorption cross-sections of n-aldehydes and unsaturated aldehydes (a);
Measured and reference value for the photolysis of unsaturated aldehydes (b).

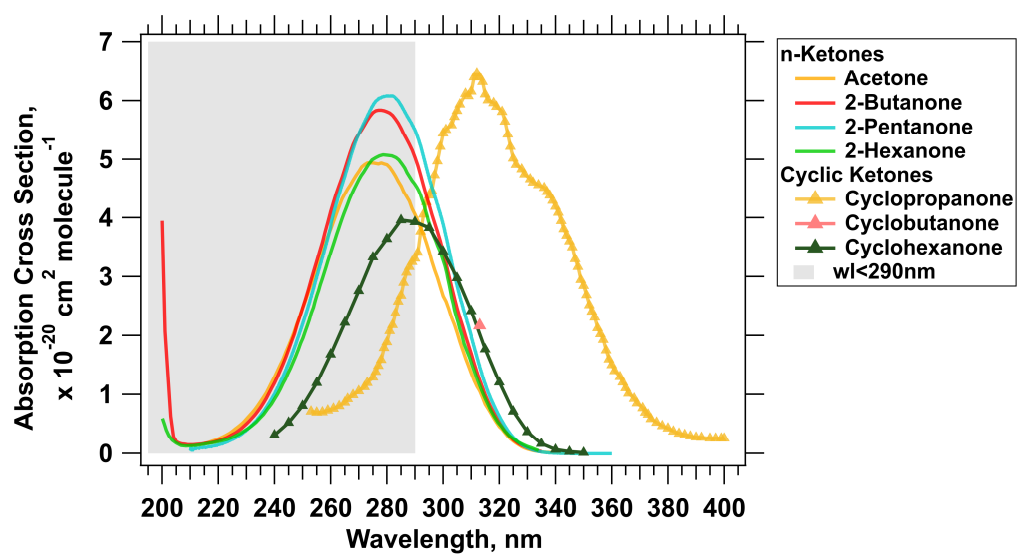


Figure S13 Comparison of the absorption spectra of n-ketones and cyclic ketones.

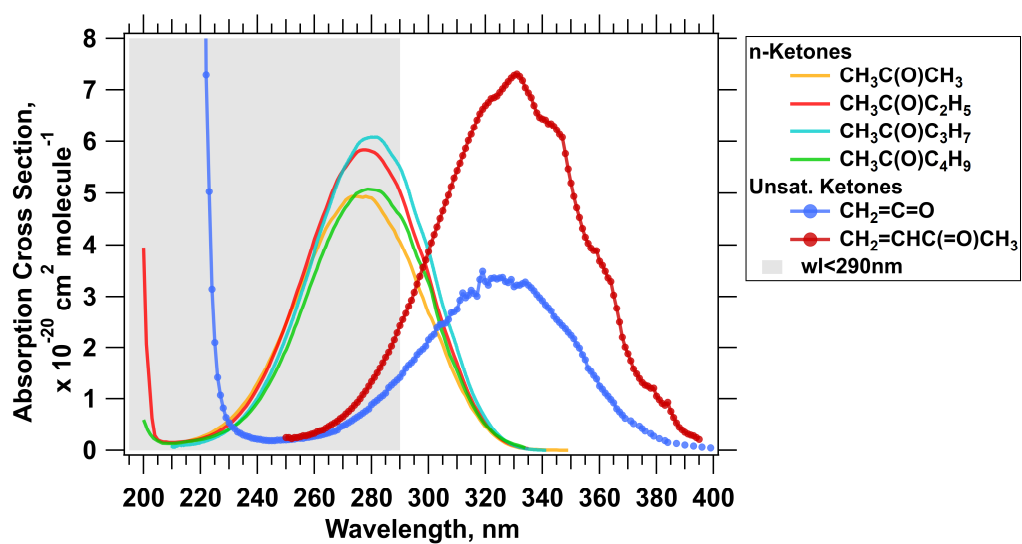


Figure S14 Absorption cross-sections of n-ketones and unsaturated ketones.

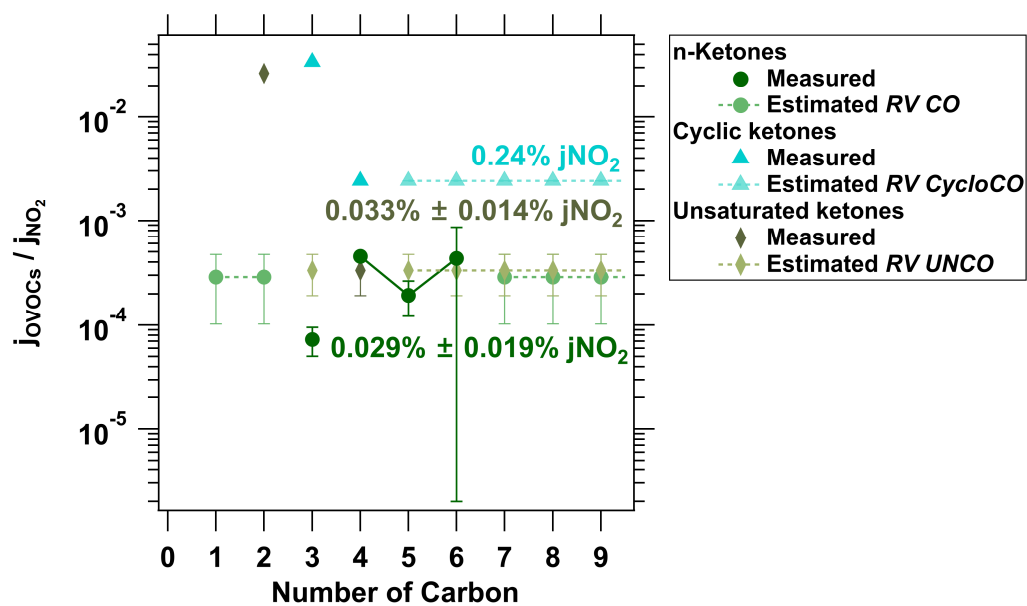


Figure S15 Measured and reference value for the photolysis of n-ketones, cyclic ketones, and unsaturated ketones.

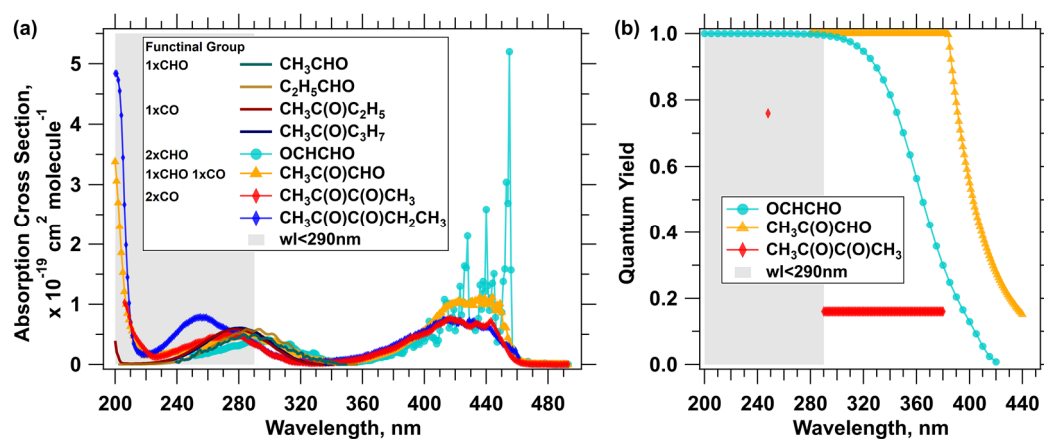
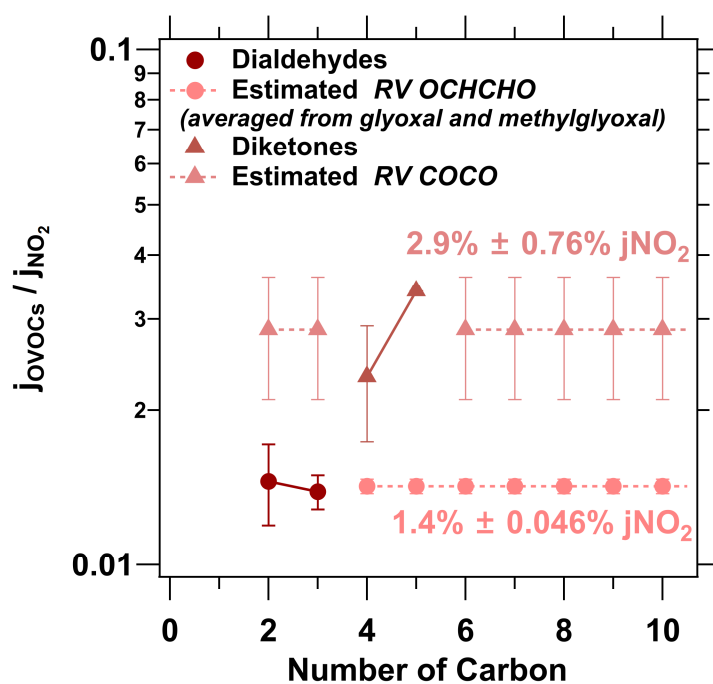


Figure S16 Absorption cross sections (a) and quantum yields (b) of ortho-dicarbonyl compounds.

710



711

712 **Figure S17** Measured and reference value for the photolysis of dialdehyde (OCHCHO)

713 and diketones (COCO).

714

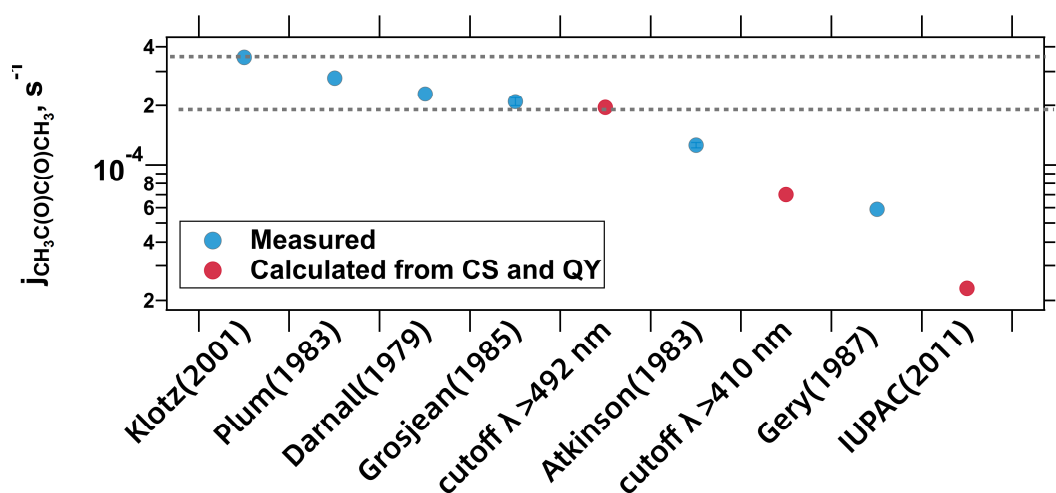


Figure S18 Photolysis rates of 2,3-butanedione reported in different studies, converted to conditions at a solar zenith angle (SZA) of 0° . The gray dashed lines indicate the reference range recommended by Calvert et al. (2011b).

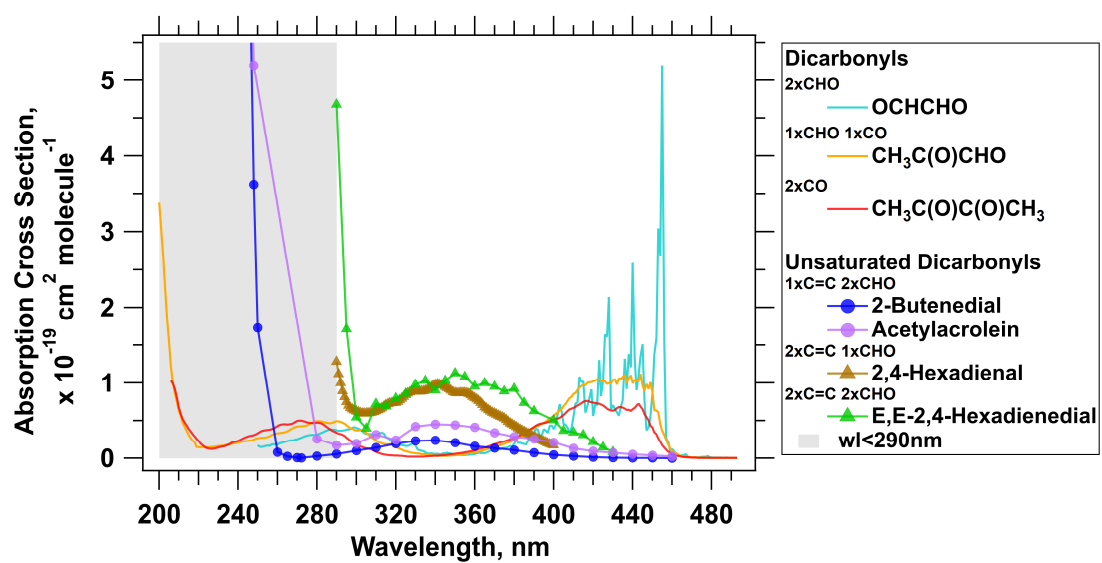


Figure S19 Absorption cross sections of saturated and unsaturated dicarbonyls.

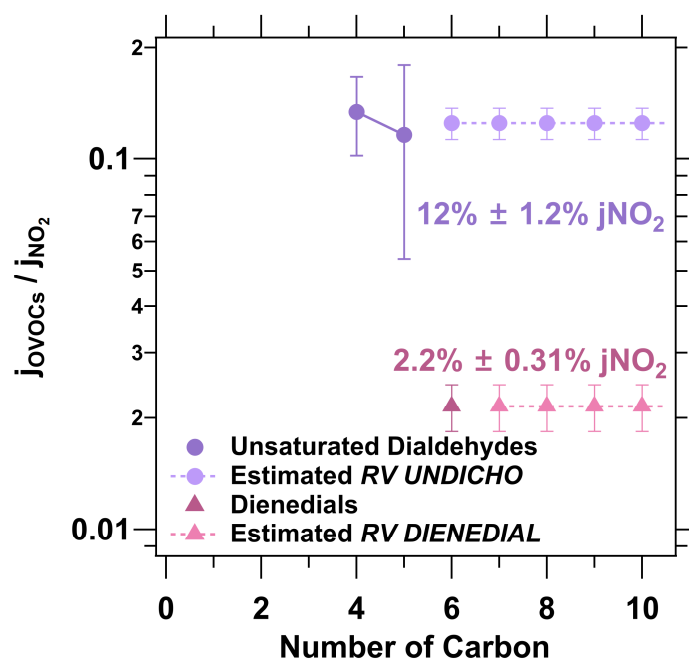


Figure S20 Measured j_{rel} and reference value of unsaturated dialdehydes and dienedials.

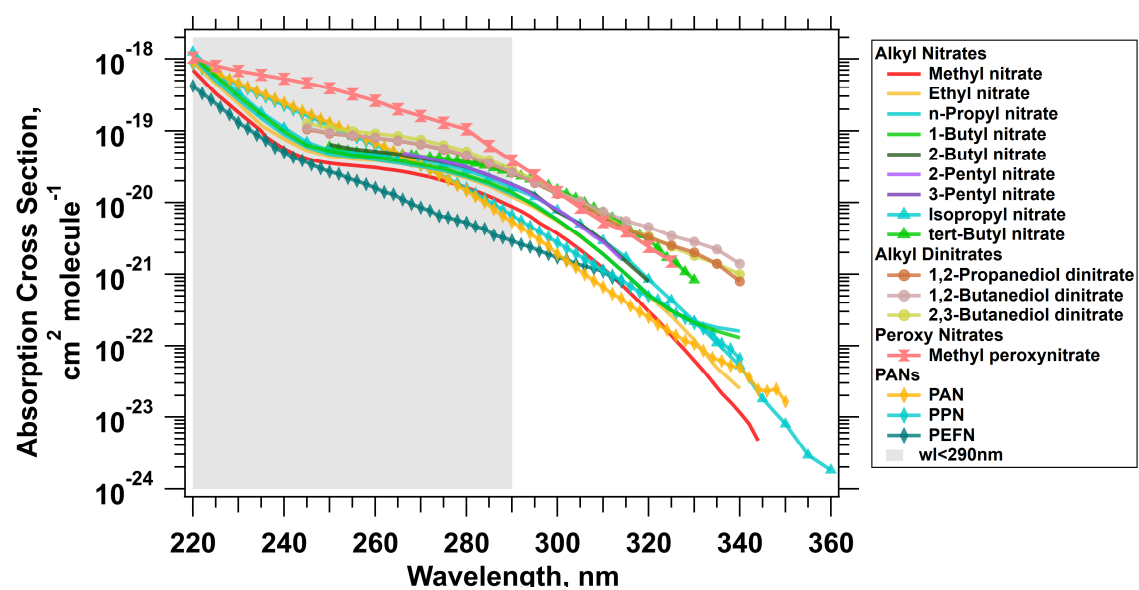


Figure S21 Comparison of absorption cross sections of alkyl nitrates, alkyl dinitrates, peroxy nitrate, and PANs.

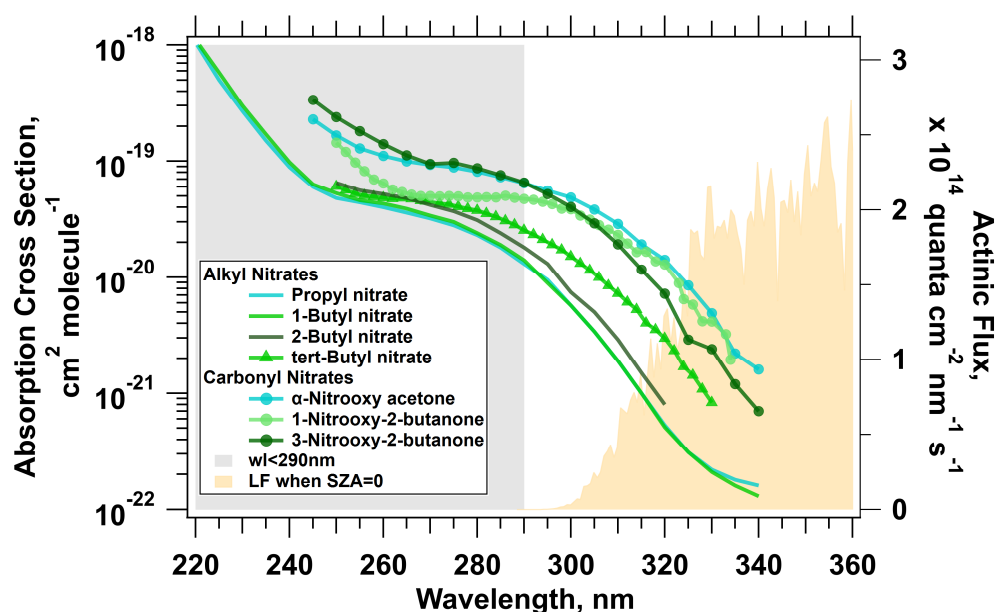


Figure S22 Comparison of absorption cross sections. The solid lines represent the absorption cross sections of alkyl nitrates containing 3 to 4 carbon atoms, while the lines with circular markers denote the absorption cross sections of carbonyl nitrates with the same carbon numbers. The light gray shaded area highlights the wavelength region below 290 nm, while the light yellow-filled area represents the actinic flux at sea level when the solar zenith angle (SZA) is 0, as calculated using the TUV model (Lantz et al., 1996; Madronich and Flocke, 1999).

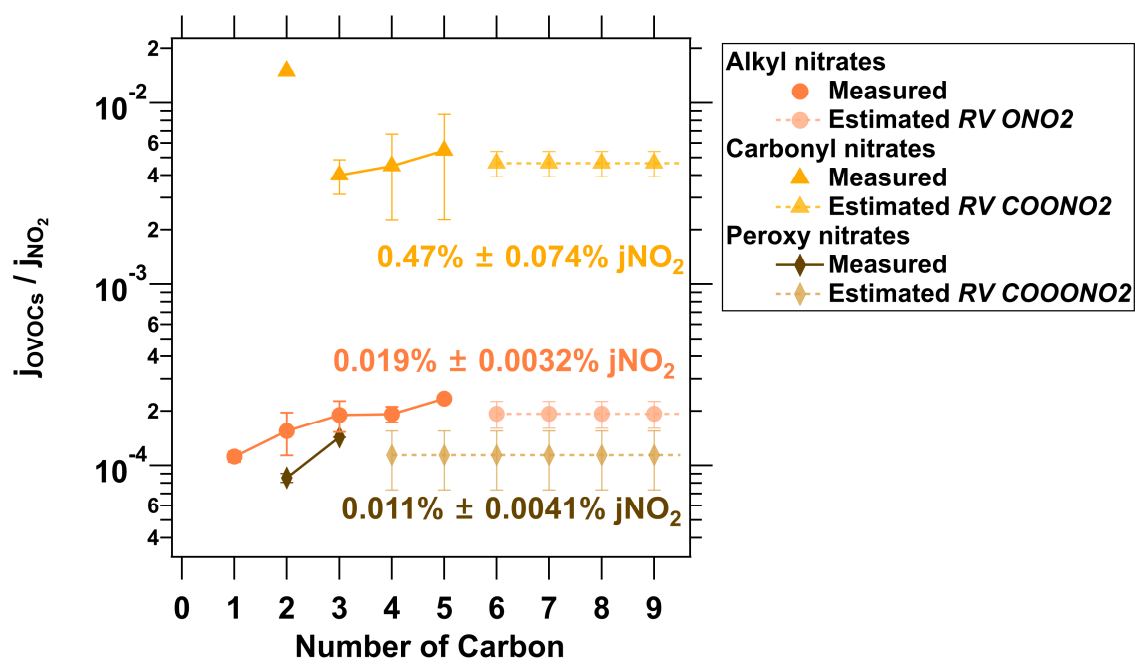


Figure S23 Measured j_{rel} and reference value of alkyl nitrates, carbonyl dinitrates, and peroxy nitrates.

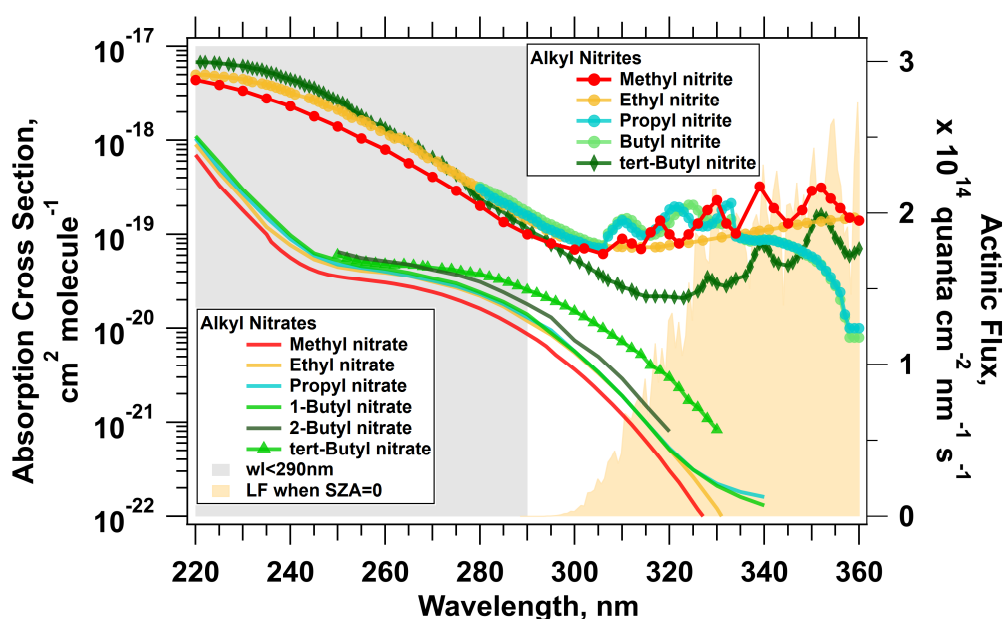


Figure S24 Comparison of absorption cross sections. The solid lines represent the absorption cross sections of alkyl nitrates containing 1 to 4 carbon atoms, while the lines with circular markers denote the absorption cross sections of alkyl nitrites with the same carbon numbers. The light gray shaded area highlights the wavelength region below 290 nm, while the light yellow-filled area represents the actinic flux at sea level when the solar zenith angle (SZA) is 0, as calculated using the TUV model (Lantz et al., 1996; Madronich and Flocke, 1999).

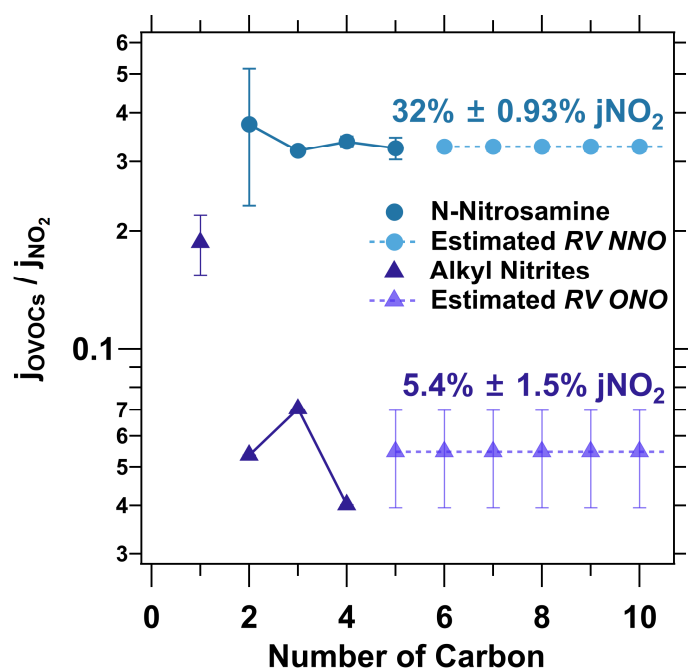


Figure S25 Measured and reference value of N-nitrosamine and alkyl nitrites.

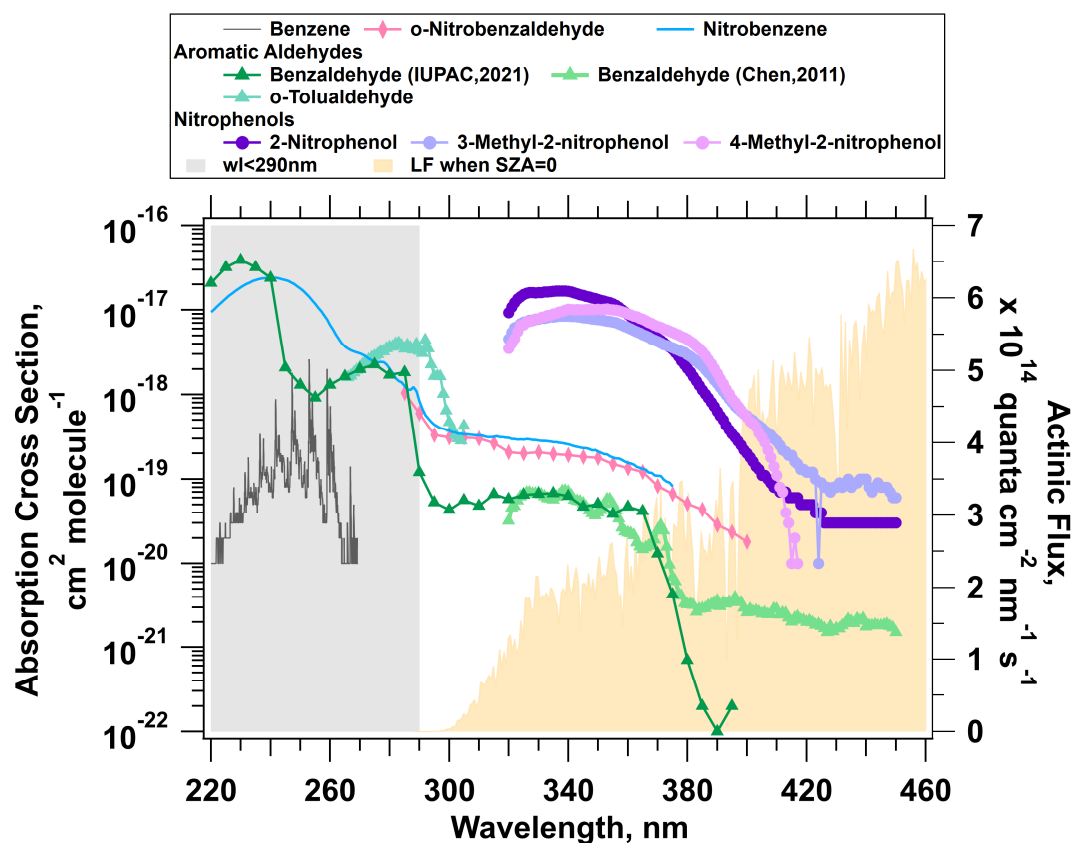


Figure S26 Comparison of absorption cross sections of benzene, nitro benzaldehyde, nitrobenzene, aromatic aldehydes, and nitrophenols. The light gray shaded area highlights the wavelength region below 290 nm, while the light yellow-filled area represents the actinic flux at sea level when the solar zenith angle (SZA) is 0.

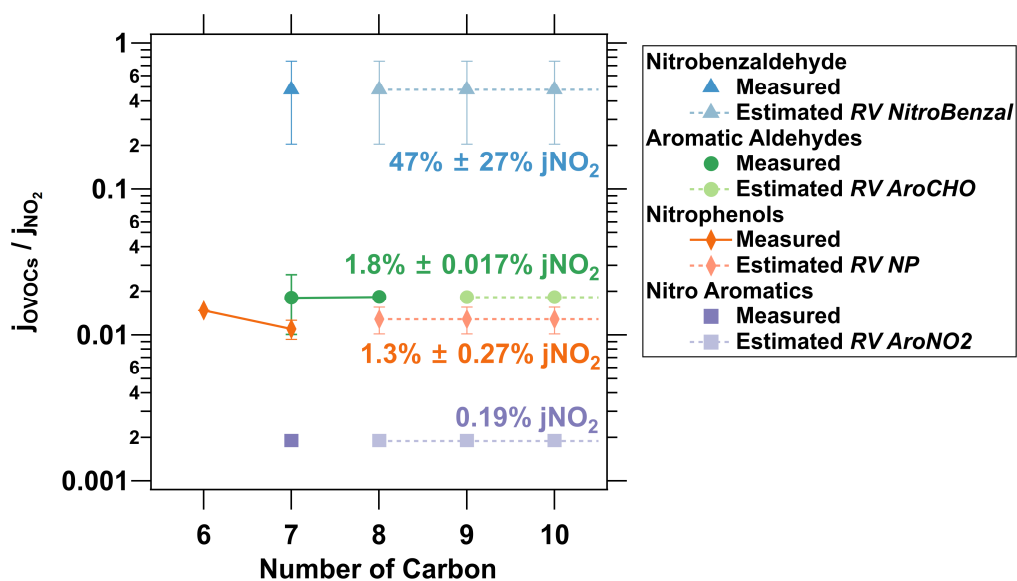


Figure S27 Measured and reference value of nitrobenzaldehyde, aromatic aldehydes, nitrophenols, and nitro aromatics compounds.

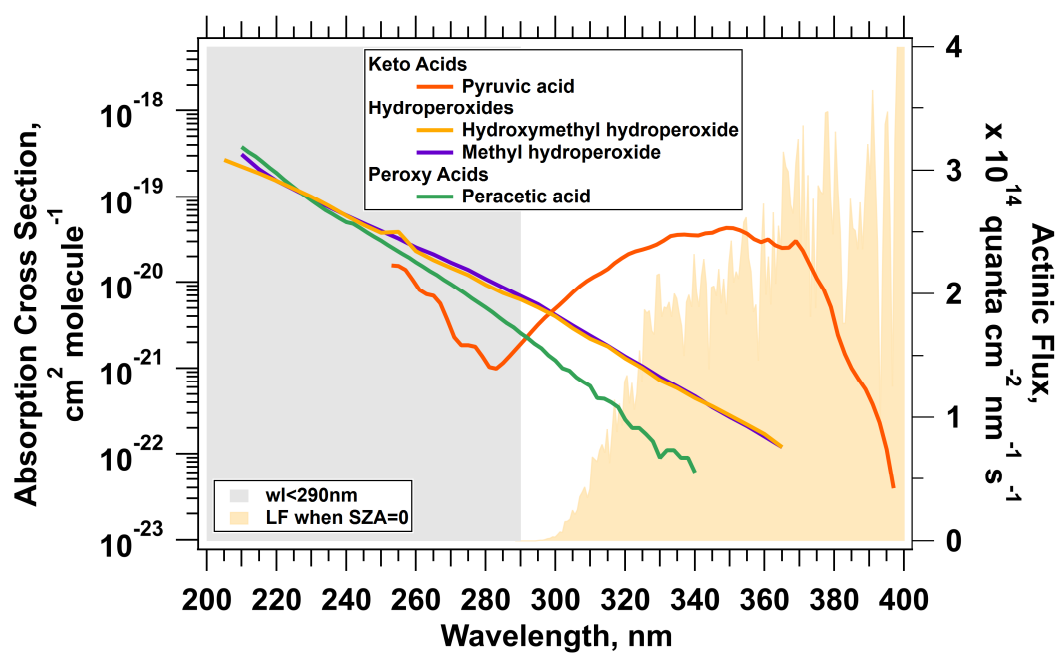


Figure S28 Comparison of absorption cross sections of keto acids, hydroperoxides, and peroxy acids. The light gray shaded area highlights the wavelength region below 290 nm, while the light yellow-filled area represents the actinic flux at sea level when the solar zenith angle (SZA) is 0.

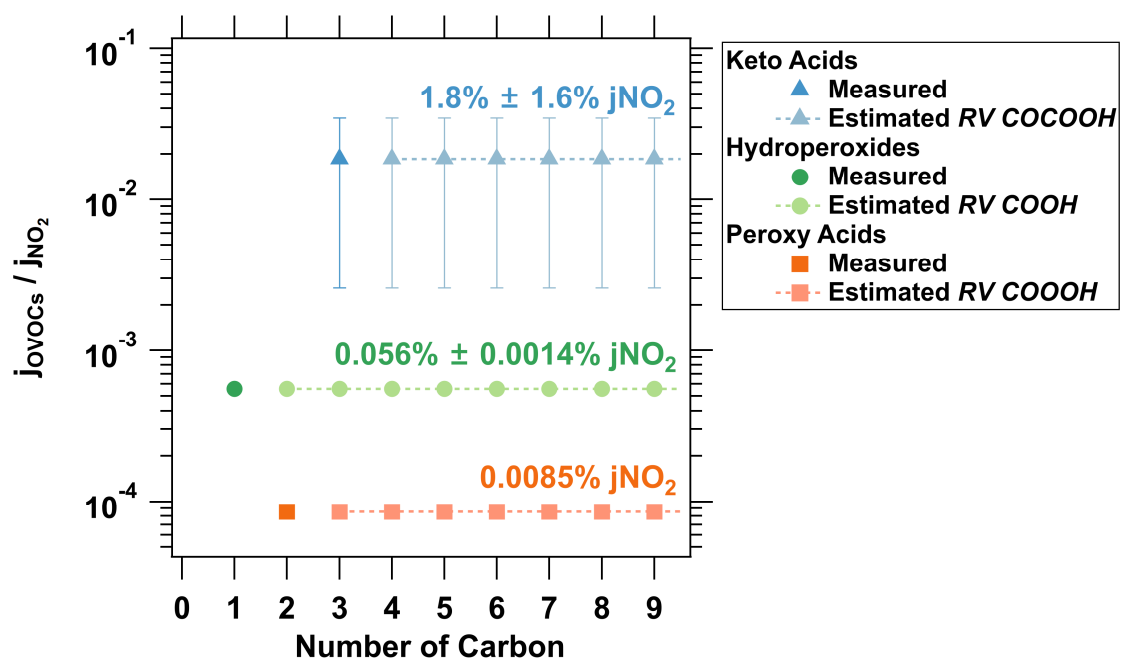


Figure S29 Measured and reference value of keto acids, hydroperoxides, and peroxy acids.

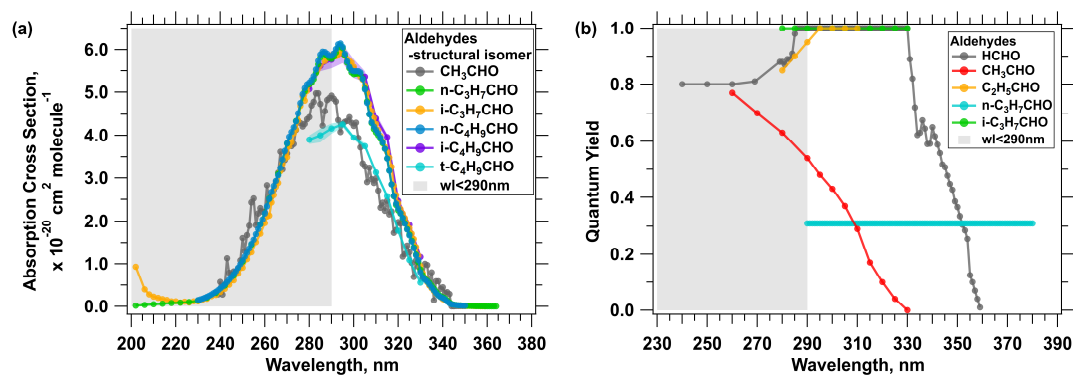


Figure S30 Comparison of absorption cross sections (a) and quantum yield (b) between n-aldehydes and branched aldehydes.

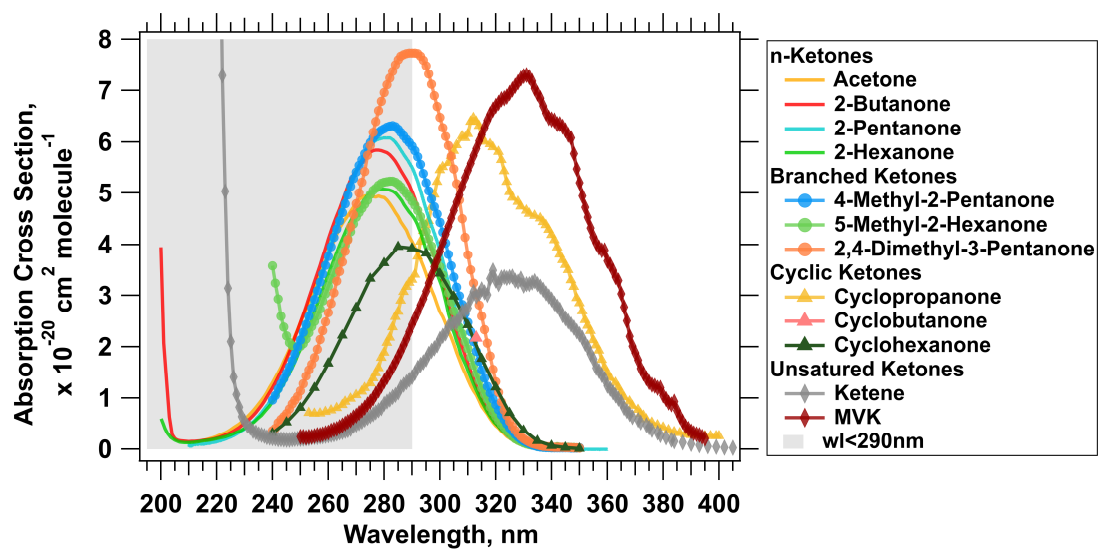


Figure S31 Comparison of absorption cross sections of n-ketones, branched ketones, cyclic ketones, and unsaturated ketones.

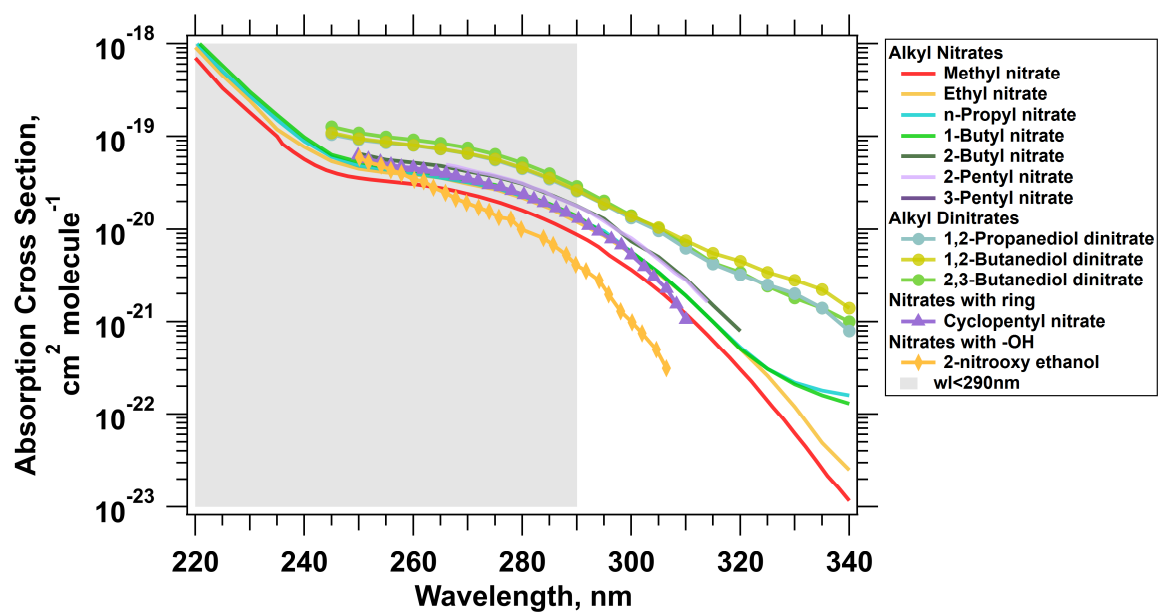


Figure S32 Comparison of absorption cross sections of alkyl nitrates, alkyl dinitrates, nitrates with ring structure, and nitrates with hydroxyl group substitution.

Table S1 Contribution of OVOC photolysis to the production rates of radicals.

Reference	Location and Time of Measurement	HCHO Photolysis, %	non-HCHO OVOCs Photolysis, %	Total, %
Contribution to p(RO_x)				
Edwards et al. (2014)	Utah, USA, winter in 2013	34	50.5	85
Heard et al. (2004)	Birmingham, England, winter in 2000	28	41	69
This study	Heshan (PRD regional), Guangdong, China, autumn in 2019	19	45.3	64
Liu et al. (2012)	Beijing, China, summer in 2007		60.6	61
Xue et al. (2016)	Hong Kong, China, summer in 2011	13 ± 3.0	41 ± 6.5	54
Volkamer et al. (2010)	Mexico City, Mexico, spring in 2003	20	33	53
Kanaya et al. (2007)	Tokyo, Japan, summer in 2004	18	30	48
This study	Guangzhou, China, autumn in 2018	16	27	43
Griffith et al. (2016)	California, USA, spring to summer in 2010	9.5 ± 0.5	32 ± 0.5	41
Li et al. (2018)	Hong Kong, China, summer to winter in 2012	19 ± 3.5	15 ± 3.6	34
Tan et al. (2019a)	Heshan (PRD regional), Guangdong, China, autumn in 2014	34		34
Michoud et al. (2012)	Palaiseau, France, summer in 2009	16	18	34
Kanaya et al. (2007)	Tokyo, Japan, winter in 2004	10	23	33
Lu et al. (2012)	Guangdong, China, summer in 2006	32 ± 4.5		32
This study	Beijing, China, summer in 2021	5.2	25	30
Tan et al. (2019b)	Four megacities in China, summer to autumn from 2014 to 2016	24 ± 9.5	4.5 ± 1.5	29
Young et al. (2012)	California, USA, spring to summer in 2010	25		25
Contribution to p(HO_x)				
Ren et al. (2013)	Texas, USA, spring in 2009	14	15	29
Ren et al. (2003)	New York, USA, summer in 2001	8.0		8.0

Reference	Location and Time of Measurement	HCHO Photolysis, %	non-HCHO OVOCs Photolysis, %	Total, %
Contribution to p(HO₂)				
Emmerson et al. (2007)	Essex, England, summer in 2003	24	73	97
Yang et al. (2018)	Beijing, China, summer in 2008		33 ± 2.0	33
Contribution to p(OH)				
Alicke et al. (2002)	Milan, Italy, spring to summer in 1998	41 ± 1.5	2.5 ± 0.5	43
Alicke et al. (2003)	Berlin, Germany, summer in 1998	37 ± 2.0		37
Elshorbany et al. (2009)	Santiago, Chile, summer in 2005	16		16
Contribution to p(RO₂)				
Yang et al. (2018)	Beijing, China, summer in 2008		74 ± 0.50	74
Emmerson et al. (2007)	Essex, England, summer in 2003		57	57
Xue et al. (2016)	Hong Kong, China, summer in 2011	13 ± 3.0	41 ± 6.5	54

789

790

791 **Table S2 All the directly measured gas species as the input of the box model in both Scenario 1 and 2.**

Trace Gases	Alkanes		Alkenes	Aromatics
NO	Ethane	n-Hexane	Isoprene	Benzene
NO ₂	Propane	2-Methylhexane	α-pinene	Ethylbenzene
O ₃	n-Butane	3-Methylhexane	β-pinene	n-Propyl benzene
CO	Iso-Butane	n-Heptane	Ethene	Iso-propyl benzene
SO ₂	2,2-Dimethylbutane	2-Methylheptane	Propene	1,2,4-Trimethylbenzene
HONO	2,3-Dimethylbutane	3-Methylheptane	1-Butene	1,3,5-Trimethylbenzene
N ₂ O ₅	n-Pentane	n-Octane	trans-2-Butene	1,2,3-Trimethylbenzene
OVOCs	Iso-Pentane	Nonane	cis-2-Butene	Toluene
Formaldehyde	2-Methylpentane	n-Decane	1-Pentene	o-Ethyl toluene
	3-Methylpentane	n-Undecane	trans-2-Pentene	m-Ethyl toluene
	2,3-Dimethylpentane	n-Dodecane	cis-2-Pentene	p-Ethyl toluene
	2,4-Dimethylpentane	Cyclohexane	1-Hexene	o-Xylene
	2,2,4-Trimethylpentane	Cyclopentane		m-Xylene
	2,3,4-Trimethylpentane	Methyl cyclopentane	Alkyne	p-Xylene
		Methyl cyclohexane	Acetylene	Styrene

792 **Table S3 20 additional non-HCHO OVOCs species constrained in Scenario 2.**

MCM Name	Species Name	MCM Name	Species Name
ACETOL	Hydroxy acetone	HOC6H4NO2	o-Nitrophenol
ACR	Acrolein	MACR	Methacrolein
BENZAL	Benzaldehyde	MEK	Methyl ethyl ketone
C2H5OH	Ethanol	MGLYOX	Methyl glyoxal
CH3CHO	Acetaldehyde	MIBK	Methyl isobutyl ketone
CH3COCH3	Acetone	MPRK	2-Pentanone
CH3COCO2H	Pyruvic acid	MVK	Methyl vinyl ketone
CH3OH	Methanol	PHENOL	Phenol
CRESOL	o-Cresol	TOL1OHNO2	2-Methyl-6-nitrophenol
ETHACET	Ethyl acetate	TOL4OHNO2	4-Methyl-2-nitrophenol

793

794

795 Table S4 Comparison of photodegradable OVOC species included in MCM, CB05, SAPRC07, RACM2, and FAST-JX mechanism.

Functional Group	Mechanism	MCM (Core Jvalue)	CB05	SAPRC07	RACM2	FAST-JX (GEOS-Chem after v10-01)
Mono-	Aldehydes	●	●	●	●	●
	Ketones	●		●	●	●
	Hydroperoxides and Peroxycarboxylic acids	●	●	●	●	●
	Nitrates	●	○	○	○	●
	Sulfate/Halogen containing	○		○		●
	PANs	●	●	●	○	●
Bi-	Unsaturated Carbonyls	●		●	●	●
	Dicarbonyls	●	●	●	●	●
	Hydroxyl ketones	○			○	●
	Carbonyl nitrates	●				○
	Hydroxyl nitrates	○				●
	Peroxyl nitrates	○				●
	Aromatic aldehydes	○		○	○	
	Nitrophenols	○		○		
Tri-	Dicarbonyl aromatics	○		○		
● Specific species ○ Lumped species or estimates based on specific species ● Both						

Table S5 Surrogate products for 714 additional photolysis reactions

Degree of Saturation (DoU)	Functional Group	Photolysis Products	Notes
/	All halogen containing species	CH ₂ CLO ₂ + HO ₂	
0	with -OOH group	BOXPROLAO + OH	
1	Contains N	C ₅ H ₂ O + NO ₂	
1	Does not contain N	CH ₃ O ₂ + HO ₂	
1.5	Ketone Carbonyl	CH ₃ O ₂ + HO ₂	
2	Contains one N	BUTALO + NO ₂	
2	Contains two N	NBUTDBO + NO ₂	
2	Does not contain N	CH ₃ O ₂ + C ₂ H ₅ CO ₃	
3	Contains one N	C ₆ H ₄ O + NO ₂	
3	Contains two N	CO ₂ N ₃ CO ₃ + NO ₂	
3	Does not contain N, contains a ring	NOPINONE + OH	
3	Does not contain N, does not contain a ring	C ₅ H ₂ O ₂ + HO ₂	
4	Contains one N	C ₇ H ₁₀ O + NO ₂	
4	Contains two N	NISOPO + HO ₂	a

Degree of Saturation (DoU)	Functional Group	Photolysis Products	Notes
4	Contains three N	INANCOCO3 + NO2	b
4	Does not contain N	C6CYTONO + OH	
5	Does not contain N, contains an aromatic ring and a carboxyl group	DM124O2 + HO2	c
5	Does not contain N, contains a non-aromatic ring structure	CH3O2 + HO2	d
5	Contains N	DMPHO + NO2	e
6	Contains N	NPHEN1O + NO2	f

797 ^a No available reference species, refer to species with DoU of 3.5 but with similar functional group instead

798 ^b No available reference species, refers to species with DoU of 5 but with same functional group

799 ^c No available reference species, structure of TM124BCO2H is used, combining the results of CH3COCO2H's photolysis products

800 ^d No available reference species, all species have a ring structure, using the result of DoU = 1

801 ^e No available reference species, structure of DMPHOHNO2 is used, combining the results of NP photolysis products

802 ^f No available reference species, structure of DNPHEN is used, combining the results of NP photolysis products

803

804 **The supplementary file includes the following datasets:**

805 1 Species Dataset – The OVOCs photolysis dataset forms the reference group, along with their references and species structural information.

806 2 Averaged Dataset – The averaged J_{rel} , $J_{overhead}$, and corresponding photolysis lifetime for 109 measured OVOCs in the reference group.

807 3 Species Used for RV – The subset of species used in the calculation of reference values.

808 4 Species Used for Coeff – The subset of species used in adjustment coefficient calculations.

809 5 Reference Value Table – A reference value dataset covering 21 categories of compounds containing 1 to 20 carbon atoms.

810 6 Prediction - MCM2327 – Predicted photolysis rates for 2327 photodegradable OVOCs included in the MCM v3.3.1 mechanism, along with
811 species information, and photolysis rates assigned in MCM. Photolysis frequencies under overhead sun are also provided for reference.

812 7 Newly Added 714 Species – A dataset of 714 newly supplemented photodegradable OVOCs in the MCM v3.3.1 mechanism, including species
813 information, predicted J_{rel} , and estimated photolysis products in the extended mechanism. Photolysis frequencies under overhead sun are also
814 provided for reference.

815

References

- Alicke, B., Platt, U., and Stutz, J.: Impact of nitrous acid photolysis on the total hydroxyl radical budget during the Limitation of Oxidant Production/Pianura Padana Produzione di Ozono study in Milan, *Journal of Geophysical Research: Atmospheres*, 107, LOP 9-1-LOP 9-17, 2002.
- Alicke, B., Geyer, A., Hofzumahaus, A., Holland, F., Konrad, S., Pätz, H., Schäfer, J., Stutz, J., Volz-Thomas, A., and Platt, U.: OH formation by HONO photolysis during the BERLIOZ experiment, *Journal of Geophysical Research: Atmospheres*, 108, PHO 3-1-PHO 3-17, 2003.
- Aruffo, E., Di Carlo, P., Dari-Salisburgo, C., Biancofiore, F., Giammaria, F., Busilacchio, M., Lee, J., Moller, S., Hopkins, J., and Punjabi, S.: Aircraft observations of the lower troposphere above a megacity: Alkyl nitrate and ozone chemistry, *Atmospheric Environment*, 94, 479-488, 2014.
- Barnes, I., Becker, K. H., and Zhu, T.: Near UV absorption spectra and photolysis products of difunctional organic nitrates: Possible importance as NO_x reservoirs, *Journal of Atmospheric Chemistry*, 17, 353-373, 1993.
- Beaver, M., Clair, J. S., Paulot, F., Spencer, K., Crounse, J., LaFranchi, B., Min, K., Pusede, S., Wooldridge, P., and Schade, G.: Importance of biogenic precursors to the budget of organic nitrates: observations of multifunctional organic nitrates by CIMS and TD-LIF during BEARPEX 2009, *Atmospheric Chemistry and Physics*, 12, 5773-5785, 2012.
- Bertram, T., Perring, A., Wooldridge, P., Dibb, J., Avery, M., and Cohen, R.: On the export of reactive nitrogen from Asia: NO_x partitioning and effects on ozone, *Atmospheric Chemistry and Physics*, 13, 4617-4630, 2013.
- Calvert, J., Mellouki, A., and Orlando, J.: Mechanisms of atmospheric oxidation of the oxygenates, Oxford University Press 2011a.
- Calvert, J. G., Mellouki, A., Orlando, J. J., Pilling, M. J., and Wallington, T. J.: Mechanisms of Photodecomposition of the Sunlight-Absorbing Oxygenates, in: Mechanisms of atmospheric oxidation of the oxygenates, Oxford University Press, 974-1357, 2011b.
- Calvert, J. G., Atkinson, R., Becker, K. H., Kamens, R. M., Seinfeld, J. H., Wallington, T. H., and Yarwood, G.: The mechanisms of atmospheric oxidation of the aromatic hydrocarbons, 2002.
- Carless, H. A. and Lee, E. K.: Photolysis and pyrolysis of 2-n-propylcyclobutanone in the gas phase, *Journal of the American Chemical Society*, 94, 1-6, 1972.
- Chen, J., Wenger, J. C., and Venables, D. S.: Near-Ultraviolet Absorption Cross Sections of Nitrophenols and Their Potential Influence on Tropospheric Oxidation Capacity, *Journal of Physical Chemistry A*, 115, 12235-12242, 10.1021/jp206929r, 2011.
- Clifford, G. M., Hadj-Aïssa, A., Healy, R. M., Mellouki, A., Muñoz, A., Wirtz, K., Martín Reviejo, M., Borrás, E., and Wenger, J. C.: The Atmospheric Photolysis of o-Tolualdehyde, *Environmental Science & Technology*, 45, 9649-9657, 10.1021/es2026533, 2011.
- Ding, X., Jiang, J., Shah, A. D., and Jung, N.: Peracetic acid emissions and exposures

- during building disinfection events, *Building and Environment*, 269, 112221, 2025.
- Edwards, P. M., Brown, S. S., Roberts, J. M., Ahmadov, R., Banta, R. M., deGouw, J. A., Dube, W. P., Field, R. A., Flynn, J. H., Gilman, J. B., Graus, M., Helmig, D., Koss, A., Langford, A. O., Lefer, B. L., Lerner, B. M., Li, R., Li, S. M., McKeen, S. A., Murphy, S. M., Parrish, D. D., Senff, C. J., Soltis, J., Stutz, J., Sweeney, C., Thompson, C. R., Trainer, M. K., Tsai, C., Veres, P. R., Washenfelder, R. A., Warneke, C., Wild, R. J., Young, C. J., Yuan, B., and Zamora, R.: High winter ozone pollution from carbonyl photolysis in an oil and gas basin, *Nature*, 514, 351-354, 10.1038/nature13767, 2014.
- Eger, P. G., Schuladen, J., Sobanski, N., Fischer, H., Karu, E., Williams, J., Riva, M., Zha, Q., Ehn, M., and Quéléver, L. L.: Pyruvic acid in the boreal forest: gas-phase mixing ratios and impact on radical chemistry, *Atmospheric Chemistry and Physics*, 20, 3697-3711, 2020.
- Elshorbany, Y. F., Kurtenbach, R., Wiesen, P., Lissi, E., Rubio, M., Villena, G., Gramsch, E., Rickard, A., Pilling, M., and Kleffmann, J.: Oxidation capacity of the city air of Santiago, Chile, *Atmospheric Chemistry and Physics*, 9, 2257-2273, 2009.
- Emmerson, K. M., Carslaw, N., Carslaw, D. C., Lee, J. D., McFiggans, G., Bloss, W. J., Gravestock, T., Heard, D. E., Hopkins, J., Ingham, T., Pilling, M. J., Smith, S. C., Jacob, M., and Monks, P. S.: Free radical modelling studies during the UK TORCH Campaign in Summer 2003, *Atmospheric Chemistry and Physics*, 7, 167-181, 10.5194/acp-7-167-2007, 2007.
- Finlayson-Pitts, B. J. and Pitts Jr, J. N.: *Chemistry of the upper and lower atmosphere: theory, experiments, and applications*, Elsevier 1999.
- Geiger, G., Stafast, H., Brühlmann, U., and Huber, J. R.: Photodissociation of dimethylnitrosamine, *Chemical Physics Letters*, 79, 525-528, 1981.
- Gierczak, T., Burkholder, J. B., Talukdar, R. K., Mellouki, A., Barone, S., and Ravishankara, A.: Atmospheric fate of methyl vinyl ketone and methacrolein, *Journal of Photochemistry and Photobiology A: Chemistry*, 110, 1-10, 1997.
- Griffith, S. M., Hansen, R., Dusanter, S., Michoud, V., Gilman, J., Kuster, W., Veres, P., Graus, M., de Gouw, J., and Roberts, J.: Measurements of hydroxyl and hydroperoxy radicals during CalNex-LA: Model comparisons and radical budgets, *Journal of Geophysical Research: Atmospheres*, 121, 4211-4232, 2016.
- Heard, D. E., Carpenter, L. J., Creasey, D. J., Hopkins, J. R., Lee, J. D., Lewis, A. C., Pilling, M. J., Seakins, P. W., Carslaw, N., and Emmerson, K. M.: High levels of the hydroxyl radical in the winter urban troposphere, *Geophysical Research Letters*, 31, 10.1029/2004gl020544, 2004.
- IUPAC: IUPAC Task Group on Atmospheric Chemical Kinetic Data Evaluation, International Union of Pure and Applied Chemistry [dataset], 2012.
- Jenkin, M. E., Young, J. C., and Rickard, A. R.: The MCM v3.3.1 degradation scheme for isoprene, *Atmospheric Chemistry and Physics*, 15, 11433-11459, 10.5194/acp-15-11433-2015, 2015.

904 Kanaya, Y., Cao, R., Akimoto, H., Fukuda, M., Komazaki, Y., Yokouchi, Y., Koike, M.,
 905 Tanimoto, H., Takegawa, N., and Kondo, Y.: Urban photochemistry in central
 906 Tokyo: 1. Observed and modeled OH and HO₂ radical concentrations during
 907 the winter and summer of 2004, *Journal of Geophysical Research:*
 908 *Atmospheres*, 112, 2007.
 909 Keller-Rudek, H., Moortgat, G. K., Sander, R., and Sørensen, R.: The MPI-Mainz
 910 UV/VIS Spectral Atlas of Gaseous Molecules of Atmospheric Interest, *Earth*
 911 *System Science Data*, 5, 365-373, 10.5194/essd-5-365-2013, 2013.
 912 Kiendler-Scharr, A., Mensah, A. A., Friese, E., Topping, D., Nemitz, E., Prévôt, A. S.,
 913 Äijälä, M., Allan, J., Canonaco, F., and Canagaratna, M.: Ubiquity of organic
 914 nitrates from nighttime chemistry in the European submicron aerosol,
 915 *Geophysical Research Letters*, 43, 7735-7744, 2016.
 916 Klotz, B., Barnes, I., and Becker, K. H.: Kinetic study of the gas-phase photolysis and
 917 OH radical reaction of E, Z-and E, E-2, 4-Hexadienedial, *International*
 918 *journal of chemical kinetics*, 31, 689-697, 1999.
 919 Klotz, B., Graedler, F., Sørensen, S., Barnes, I., and Becker, K. H.: A kinetic study of
 920 the atmospheric photolysis of α -dicarbonyls, *International Journal of*
 921 *Chemical Kinetics*, 33, 9-20, 2001.
 922 Lantz, K. O., Shetter, R. E., Cantrell, C. A., Flocke, S. J., Calvert, J. G., and Madronich,
 923 S.: Theoretical, actinometric, and radiometric determinations of the
 924 photolysis rate coefficient of NO₂ during the Mauna Loa Observatory
 925 Photochemistry Experiment 2, *Journal of Geophysical Research:*
 926 *Atmospheres*, 101, 14613-14630, <https://doi.org/10.1029/96JD00215>, 1996.
 927 Li, Z., Xue, L., Yang, X., Zha, Q., Tham, Y. J., Yan, C., Louie, P. K., Luk, C. W., Wang,
 928 T., and Wang, W.: Oxidizing capacity of the rural atmosphere in Hong Kong,
 929 Southern China, *Science of the total environment*, 612, 1114-1122, 2018.
 930 Liu, Z., Nguyen, V. S., Harvey, J., Müller, J.-F., and Peeters, J.: The photolysis of α -
 931 hydroperoxycarbonyls, *Physical Chemistry Chemical Physics*, 20, 6970-
 932 6979, 10.1039/c7cp08421h, 2018.
 933 Liu, Z., Wang, Y., Gu, D., Zhao, C., Huey, L. G., Stickel, R., Liao, J., Shao, M., Zhu,
 934 T., and Zeng, L.: Summertime photochemistry during CAREBeijing-2007:
 935 ROx budgets and O₃ formation, *Atmospheric Chemistry and Physics*, 12,
 936 7737-7752, 2012.
 937 Lu, K. D., Rohrer, F., Holland, F., Fuchs, H., Bohn, B., Brauers, T., Chang, C. C.,
 938 Haseler, R., Hu, M., Kita, K., Kondo, Y., Li, X., Lou, S. R., Nehr, S., Shao,
 939 M., Zeng, L. M., Wahner, A., Zhang, Y. H., and Hofzumahaus, A.:
 940 Observation and modelling of OH and HO₂ concentrations in the Pearl River
 941 Delta 2006: a missing OH source in a VOC rich atmosphere, *Atmospheric*
 942 *Chemistry and Physics*, 12, 1541-1569, 10.5194/acp-12-1541-2012, 2012.
 943 Madronich, S. and Flocke, S.: The role of solar radiation in atmospheric chemistry, in:
 944 *Environmental Photochemistry*, 1 ed., edited by: Boule, P., Springer Berlin,
 945 Heidelberg, 1-26, https://10.1007/978-3-540-69044-3_1, 1999.
 946 Mellouki, A., Ammann, M., Cox, R. A., Crowley, J. N., Herrmann, H., Jenkin, M. E.,
 947 McNeill, V. F., Troe, J., and Wallington, T. J.: Evaluated kinetic and

948 photochemical data for atmospheric chemistry: volume VIII—gas-phase
 949 reactions of organic species with four, or more, carbon atoms ($\geq C_4$),
 950 Atmospheric Chemistry and Physics, 21, 4797-4808, 2021.
 951 Michoud, V., Kukui, A., Camredon, M., Colomb, A., Borbon, A., Miet, K., Aumont, B.,
 952 Beekmann, M., Durand-Jolibois, R., and Perrier, S.: Radical budget analysis
 953 in a suburban European site during the MEGAPOLI summer field campaign,
 954 Atmospheric Chemistry and Physics, 12, 11951-11974, 2012.
 955 Müller, J. F., Peeters, J., and Stavrou, T.: Fast photolysis of carbonyl nitrates from
 956 isoprene, Atmospheric Chemistry and Physics, 14, 2497-2508, 10.5194/acp-
 957 14-2497-2014, 2014.
 958 Nakashima, K., Uchida-Kai, K., Koyanagi, M., and Kanda, Y.: Solvent effects on the
 959 intensities of forbidden bands of molecules. Absorption spectra of acetone
 960 and cyclopentanone, Bulletin of the Chemical Society of Japan, 55, 415-419,
 961 1982.
 962 Newland, M. J., Rea, G. J., Thuner, L. P., Henderson, A. P., Golding, B. T., Rickard, A.
 963 R., Barnes, I., and Wenger, J.: Photochemistry of 2-butenedial and 4-oxo-2-
 964 pentenal under atmospheric boundary layer conditions, Phys Chem Chem
 965 Phys, 21, 1160-1171, 10.1039/c8cp06437g, 2019.
 966 Nielsen, C. J., Herrmann, H., and Weller, C.: Atmospheric chemistry and environmental
 967 impact of the use of amines in carbon capture and storage (CCS), Chemical
 968 Society Reviews, 41, 6684-6704, 2012.
 969 Orlando, J. J. and Tyndall, G. S.: Gas phase UV absorption spectra for peracetic acid,
 970 and for acetic acid monomers and dimers, Journal of Photochemistry and
 971 Photobiology A: Chemistry, 157, 161-166, 2003.
 972 Reed Harris, A. E., Cazaunau, M., Gratien, A., Pangui, E., Doussin, J.-F. o., and Vaida,
 973 V.: Atmospheric simulation chamber studies of the gas-phase photolysis of
 974 pyruvic acid, The Journal of Physical Chemistry A, 121, 8348-8358, 2017.
 975 Ren, X., Harder, H., Martinez, M., Leshner, R. L., Oliger, A., Simpasa, J. B., Brune, W.
 976 H., Schwab, J. J., Demerjian, K. L., and He, Y.: OH and HO₂ chemistry in the
 977 urban atmosphere of New York City, Atmospheric Environment, 37, 3639-
 978 3651, 2003.
 979 Ren, X., Van Duin, D., Cazorla, M., Chen, S., Mao, J., Zhang, L., Brune, W. H., Flynn,
 980 J. H., Grossberg, N., and Lefer, B. L.: Atmospheric oxidation chemistry and
 981 ozone production: Results from SHARP 2009 in Houston, Texas, Journal of
 982 Geophysical Research: Atmospheres, 118, 5770-5780, 2013.
 983 Rossignol, S., Aregahegn, K. Z., Tinel, L., Fine, L., Nozière, B., and George, C.:
 984 Glyoxal induced atmospheric photosensitized chemistry leading to organic
 985 aerosol growth, Environmental science & technology, 48, 3218-3227, 2014.
 986 Sander, S., Friedl, R., Abbatt, J., Barker, J., Burkholder, J., Golden, D., Kolb, C., Kurylo,
 987 M., Moortgat, G., and Wine, P.: Chemical kinetics and photochemical data
 988 for use in atmospheric studies, evaluation number 14, JPL publication, 10,
 989 2011.
 990 Sekimoto, K., Li, S.-M., Yuan, B., Koss, A., Coggon, M., Warneke, C., and de Gouw,
 991 J.: Calculation of the sensitivity of proton-transfer-reaction mass

spectrometry (PTR-MS) for organic trace gases using molecular properties, International Journal of Mass Spectrometry, 421, 71-94, 2017.

Simpson, I. J., Meinardi, S., Blake, D. R., Blake, N. J., Rowland, F. S., Atlas, E., and Flocke, F.: A biomass burning source of C1–C4 alkyl nitrates, Geophysical research letters, 29, 21-21-21-24, 2002.

Tadić, J., Moortgat, G. K., and Wirtz, K.: Photolysis of glyoxal in air, Journal of Photochemistry and Photobiology A: Chemistry, 177, 116-124, 2006.

Tan, Z., Lu, K., Hofzumahaus, A., Fuchs, H., Bohn, B., Holland, F., Liu, Y., Rohrer, F., Shao, M., and Sun, K.: Experimental budgets of OH, HO₂, and RO₂ radicals and implications for ozone formation in the Pearl River Delta in China 2014, Atmospheric chemistry and physics, 19, 7129-7150, 2019a.

Tan, Z., Lu, K., Jiang, M., Su, R., Wang, H., Lou, S., Fu, Q., Zhai, C., Tan, Q., and Yue, D.: Daytime atmospheric oxidation capacity in four Chinese megacities during the photochemically polluted season: a case study based on box model simulation, Atmospheric Chemistry and Physics, 19, 3493-3513, 2019b.

Tomas, A., Aslan, L., Muñoz, A., Ródenas, M., Vera, T., Borrás, E., Coddeville, P., and Fittschen, C.: Photolysis of multifunctional carbonyl compounds under natural irradiation at EUPHORE, Atmospheric Environment, 253, 118352, 10.1016/j.atmosenv.2021.118352, 2021.

Tuazon, E., Atkinson, R., Aschmann, S., and Arey, J.: Kinetics and products of the gas-phase reactions of O₃ with amines and related compounds, Research on chemical intermediates, 20, 303-320, 1994.

Volkamer, R., Sheehy, P., Molina, L. T., and Molina, M. J.: Oxidative capacity of the Mexico City atmosphere–Part 1: A radical source perspective, Atmospheric Chemistry and Physics, 10, 6969-6991, 2010.

Wade, E. A., Mellinger, A., Hall, M. A., and Moore, C. B.: How a transition state tightens: the singlet photodissociation of ketene as a test case, The Journal of Physical Chemistry A, 101, 6568-6576, 1997a.

Wade, E. A., Clauberg, H., Kim, S. K., Mellinger, A., and Moore, C. B.: Dynamics of rotational energy release for dissociation of singlet ketene and the singlet/triplet branching ratio, The Journal of Physical Chemistry A, 101, 732-739, 1997b.

Wang, H., Peng, C., Wang, X., Lou, S., Lu, K., Gan, G., Jia, X., Chen, X., Chen, J., and Wang, H.: N₂O₅ uptake onto saline mineral dust: a potential missing source of tropospheric ClNO₂ in inland China, Atmospheric Chemistry and Physics, 22, 1845-1859, 2022.

Wang, Z., Yuan, B., Ye, C., Roberts, J., Wisthaler, A., Lin, Y., Li, T., Wu, C., Peng, Y., Wang, C., Wang, S., Yang, S., Wang, B., Qi, J., Wang, C., Song, W., Hu, W., Wang, X., Xu, W., Ma, N., Kuang, Y., Tao, J., Zhang, Z., Su, H., Cheng, Y., Wang, X., and Shao, M.: High Concentrations of Atmospheric Isocyanic Acid (HNCO) Produced from Secondary Sources in China, Environmental Science & Technology, 54, 11818-11826, 10.1021/acs.est.0c02843, 2020.

Wild, O., Zhu, X., and Prather, M. J.: Fast-J: Accurate simulation of in-and below-cloud photolysis in tropospheric chemical models, Journal of Atmospheric

- Chemistry, 37, 245-282, 2000.
- Wu, C., Wang, C., Wang, S., Wang, W., Yuan, B., Qi, J., Wang, B., Wang, H., Wang, C., Song, W., Wang, X., Hu, W., Lou, S., Ye, C., Peng, Y., Wang, Z., Huangfu, Y., Xie, Y., Zhu, M., Zheng, J., Wang, X., Jiang, B., Zhang, Z., and Shao, M.: Measurement report: Important contributions of oxygenated compounds to emissions and chemistry of volatile organic compounds in urban air, *Atmospheric Chemistry and Physics*, 20, 14769-14785, 10.5194/acp-20-14769-2020, 2020.
- Xiang, B. and Zhu, L.: Absorption cross sections of E, E-2, 4-hexadienedial at 248 nm, and in the 290–430 nm region, and photolysis study at 248, 308, and 351 nm, *Chemical Physics Letters*, 450, 31-38, 2007.
- Xue, L., Gu, R., Wang, T., Wang, X., Saunders, S., Blake, D., Louie, P. K., Luk, C. W., Simpson, I., and Xu, Z.: Oxidative capacity and radical chemistry in the polluted atmosphere of Hong Kong and Pearl River Delta region: analysis of a severe photochemical smog episode, *Atmospheric Chemistry and Physics*, 16, 9891-9903, 2016.
- Yang, Q., Su, H., Li, X., Cheng, Y., Lu, K., Cheng, P., Gu, J., Guo, S., Hu, M., and Zeng, L.: Daytime HONO formation in the suburban area of the megacity Beijing, China, *Science China Chemistry*, 57, 1032-1042, 2014.
- Yang, X., Xue, L., Wang, T., Wang, X., Gao, J., Lee, S., Blake, D. R., Chai, F., and Wang, W.: Observations and explicit modeling of summertime carbonyl formation in Beijing: identification of key precursor species and their impact on atmospheric oxidation chemistry, *Journal of Geophysical Research: Atmospheres*, 123, 1426-1440, 2018.
- Yarwood, G., Rao, S., Yocke, M., and Whitten, G.: Updates to the carbon bond chemical mechanism: CB05 final report to the US EPA, Rt-0400675, 2005.
- Ye, C., Yuan, B., Lin, Y., Wang, Z., Hu, W., Li, T., Chen, W., Wu, C., Wang, C., Huang, S., Qi, J., Wang, B., Wang, C., Song, W., Wang, X., Zheng, E., Krechmer, J. E., Ye, P., Zhang, Z., Wang, X., Worsnop, D. R., and Shao, M.: Chemical characterization of oxygenated organic compounds in the gas phase and particle phase using iodide CIMS with FIGAERO in urban air, *Atmospheric Chemistry and Physics*, 21, 8455-8478, 10.5194/acp-21-8455-2021, 2021.
- Young, C. J., Washenfelder, R. A., Roberts, J. M., Mielke, L. H., Osthoff, H. D., Tsai, C., Pikelnaya, O., Stutz, J., Veres, P. R., and Cochran, A. K.: Vertically resolved measurements of nighttime radical reservoirs in Los Angeles and their contribution to the urban radical budget, *Environmental science & technology*, 46, 10965-10973, 2012.
- Yu, Y., Cheng, P., Li, H., Yang, W., Han, B., Song, W., Hu, W., Wang, X., Yuan, B., and Shao, M.: Budget of nitrous acid (HONO) and its impacts on atmospheric oxidation capacity at an urban site in the fall season of Guangzhou, China, *Atmospheric Chemistry and Physics Discussions*, 2021, 1-38, 2021.
- Zhang, Y., Cao, F., Fan, M.-Y., Xiang, Y.-K., Li, H.-Y., Xue, Y.-W., and Zhang, Y.-L.: Atmospheric HONO Concentration Levels and Generation Mechanisms in Nanjing in Winter and Summer, *Environmental Science*, 45, 6286-6293, 2024.